CORROSION BEHAVIOUR OF POLY-L-LACTIC ACID COATED MAGNESIUM BY ELECTROSPINNING

WAN NUR ATIKAH BINTI HAJI WAN NAFI

FACULTY OF ENGINEERING
UNIVERSITY OF MALAYA
KUALA LUMPUR

2017

CORROSION BEHAVIOUR OF POLY-L-LACTIC ACID COATED MAGNESIUM BY ELECTROSPINNING

WAN NUR ATIKAH BINTI HAJI WAN NAFI

DISSERTATION SUBMITTED IN FULFILMENT OF THE REQUIREMENTS FOR THE DEGREE OF MASTER OF ENGINEERING SCIENCE

FACULTY OF ENGINEERING
UNIVERSITY OF MALAYA
KUALA LUMPUR

2017

UNIVERSITY OF MALAYA

ORIGINAL LITERARY WORK DECLARATION

Name of Candidate: Wan Nur Atikah Binti Haji Wan Nafi

Matric No: KGA 130062

Name of Degree: Master of Engineering Science

Title of Dissertation ("this Work"):

CORROSION BEHAVIOUR OF POLY-L-LACTIC ACID COATED

MAGNESIUM BY ELECTROSPINNING

Field of Study: Materials science and engineering

I do solemnly and sincerely declare that:

(1) I am the sole author/writer of this Work;
(2) This Work is original;
(3) Any use of any work in which copyright exists was done by way of fair dealing and for permitted purposes and any excerpt or extract from, or reference to or reproduction of any copyright work has been disclosed expressly and sufficiently and the title of the Work and its authorship have been acknowledged in this Work;
(4) I do not have any actual knowledge nor do I ought reasonably to know that the making of this work constitutes an infringement of any copyright work;
(5) I hereby assign all and every rights in the copyright to this Work to the University of Malaya ("UM"), who henceforth shall be owner of the copyright in this Work and that any reproduction or use in any form or by any means whatsoever is prohibited without the written consent of UM having been first had and obtained;
(6) I am fully aware that if in the course of making this Work I have infringed any copyright whether intentionally or otherwise, I may be subject to legal action or any other action as may be determined by UM.

Candidate's Signature Date:

Subscribed and solemnly declared before,

Witness's Signature Date:

Name:

Designation:

CORROSION BEHAVIOUR OF POLY-L-LACTIC ACID COATED MAGNESIUM BY ELECTROSPINNING

ABSTRACT

Every year, the rate of accident involving bone fractures increases rapidly and most fractures need to be fixed with surgical bone implants. Most implants are made from medical grade metal such as stainless steel, cobalt, titanium and others. One of the characters of a good short term implant is its ability to be degraded after bones have healed. However, most of the temporary implants are made from non-biodegradable metals. In consequence, magnesium alloys has potential to be used as short term implants due to their ability to degrade in chloride containing solution and properties similar to human bones. However, its high degradation rate limits its clinical applications. This study has introduced an approach to control the corrosion rate of high purity magnesium (HP Mg) and AZ91 by coating them with polymeric membrane of poly-L-lactic acid (PLLA) by electrospinning. An 8 wt % of PLLA was magnetic stirred to dissolve in the chloroform at room temperature. The prepared PLLA solution was then fed into a 10 ml syringe with thin needle. The electrospun coating of PLLA on HP Mg and AZ91 samples were done at feed rate of 1 ml/hr, voltage of 10 kV and distance of 15 cm between the syringe tip and collector. Scanning electron microscope (SEM) and microscratch test were done to characterize the thickness and adhesiveness of the coating on HP Mg and AZ91. In addition ASTM 3359 standard test and surface profiler were also performed to study the adhesiveness and thickness of the coating respectively. The corrosion behaviour of uncoated Mg and Mg coated PLLA samples were studied by immersing them in Hank's solution for 14 days at human body temperature (37 °C). The pH of Hank's solution was maintained at 7. The corrosion rate was calculated from evolved hydrogen during the immersion and weight loss after immersion. The surface of the samples before and after immersion was evaluated by scanning electron microscope

(SEM). It was observed that PLLA was successfully coated the HP Mg and AZ91 samples. The corrosion rates of HP Mg and AZ91 coated PLLA samples without hole were found lower than uncoated samples. PLLA coating on HP Mg and AZ91 by electrospinning has improved the corrosion resistance by delaying the corrosion initiation.

Keywords: Magnesium, PLLA coating, Hydrogen Evolution, Weight loss, SEM

KAKISAN OLEH MAGNESIUM BERSALUT POLI-L-LAKTIK ASID DARIPADA PUTARAN ELEKTRON

ABSTRAK

Setiap tahun, kadar kemalangan yang melibatkan patah tulang meningkat dengan cepat dan ia boleh dipulihkan dengan pembedahan melibatkan implan. Kebanyakan implan diperbuat daripada logam gred perubatan seperti keluli tahan karat, kobalt, titanium dan sebagainya. Salah satu ciri implan untuk masa yang singkat yang bagus adalah keupayaannya untuk terurai selepas tulang telah sembuh. Walaubagaimanapun, kebanyakan implan untuk tempoh masa yang singkat diperbuat daripada bahan bukan biodegradasi. Oleh itu, magnesium aloi mempunyai potensi untuk digunakan sebagai implan untuk masa yang singkat kerana kemampuannya untuk terurai di dalam cecair berklorida dan mempunyai ciri yang sama seperti tulang manusia. Namun begitu, kadar kakisannya yang tinggi telah menghalang aplikasi klinikal. Kajian ini memperkenalkan pendekatan untuk mengawal kadar kakisan pada magnesium berketumpatan tinggi (HP Mg) dan AZ91 dengan menyalutinya dengan lapisan membran polimer oleh poli-L-laktik asid (PLLA) melalui proses putaran elektron. 8 wt% daripada PLLA dikacau dengan magnet untuk terlarut di dalam kloroform pada suhu bilik. Kemudian, bancuhan PLLA yang telah disediakan diisi kedalam 10 ml picagari yang bersama jarum. Salutan PLLA ke atas HP Mg dan AZ91 melalui putaran elektron dilakukan dengan kadar suapan pada 1 ml/hr, voltan 10 kV dan 15 cm adalah jarak antara hujung picagari dan pemungut. Imbasan mikroskop elektron (SEM) dan ujian cakaran mikro telah digunakan untuk mengenal pasti ketebalan dan kelekatan salutan pada HP Mg dan AZ91. Tambahan pula ASTM 3359 ujian standard dan profil permukaan juga digunakan untuk menguji kelekatan dan ketebalan salutan tersebut. Kadar kakisan sampel Mg tidak bersalut dan Mg bersalut PLLA diuji dengan ujian rendaman dalam bendalir manusia biologi (bendalir Hank) selama 14 hari pada suhu badan manusia (37

°C). pH bendalir Hank dikekalkan pada 7. Kelakuan kakisan diukur melalui pengeluaran hydrogen semasa rendaman dan penurunan berat adalah selepas rendaman. Permukaan sampel sebelum dan selepas rendalam dikenal pasti menggunakan imbasan mikroskop elektron (SEM). Hasil pemerhatian, PLLA berjaya menyaluti sampel HP Mg dan AZ91. Kadar kakisan sampel HP Mg dan AZ91 yang bersalut tanpa lubang dipercayai lebih rendah berbanding sampel tidak berbalut. Salutan PLLA pada HP Mg dan AZ91 menggunakan putaran elektron telah meningkatkan pertahanan kakisan seterusnya memperlahankan permulaan kakisan.

Kata kunci: Magnesium, Salutan PLLA , Pengeluaran Hidrogen, Penurunan berat, SEM

ACKNOWLEDGEMENTS

First of all, praise to Allah for his wisdom and for giving me the strength and patience to complete my master dissertation project.

Secondly, I wish to expand my utmost gratitude to my supervisors, Prof. Madya Dr. Amalina M. Afifi and Dr. Nor Ishida Zainal Abidin for accepting me as a Master student and for all of the guidance they provided throughout my Master study. Their guidance helped me in all the time of research and writing of this thesis.

Besides my supervisors, I would like to thank the rest of my labmates for their kindness, constructive suggestions, motivation, and inputs that contributed to my research work. My sincere thanks also go to the staff of the Department of Mechanical, Faculty of Engineering, University of Malaya for their help and informative knowledge.

Last but not the least, I would like to extend my gratitude to my family and friends for their constant support, motivation and supporting me spiritually throughout my life.

TABLE OF CONTENTS

LIST OF FIGURES

LIST OF TABLES

LIST OF SYMBOLS AND ABBREVIATIONS

Mg	: Magnesium
PLLA	: poly(L-lactic acid)
HP Mg	: High Purity Magnesium
CO_2	: Carbon dioxide
Ti	: Titanium
Mg-Cd	: Magnesium-Cadmium
Co-Cr	: Cobalt-Chromium
ECM	: Extracellular Matrix
PCL	: poly(ε-caprolactone)
PGA	: poly(glycolic acid)
PLGA	: poly(lactic-co-glycolic acid)
FDA	: Food and Drug Administration
H_2	: Hydrogen
H_2O	: Water
Fe	: Ferum
Ni	: Nickel
Cu	: Copper
$Mg(OH)_2$	: Magnesium Hydroxide
ID	: Inner diameter
OD	: Outer diameter
SEM	: Scanning Electron Microscope
EDX	: Energy dispersive X-ray spectroscopy
FESEM	: Field-emission scanning electron microscopy
XRD	: X-ray diffraction

FTIR : Fourier Transform Infrared

XRF : X-ray fluorescence spectroscopy

AZ91 : Magnesium alloys

PLLA-HP Mg : HP Mg coated with PLLA

PLLA-AZ91 : AZ91 coated with PLLA

ASTM : American Standard Test Method

SiC : Silicon carbide

W_L : Weight loss rate

Pw : Corrosion rate based on weight loss

P_{AH} : Corrosion rate based on hydrogen evolution volume

Wb : Weight before

Wa : Weight after

ρ : Density

Al : Aluminium

2Θ : 2 thetha

C : Carbon

O : Oxygen

Zn : Zinc

Ca/P : Calcium/Phosphate

CHAPTER 1: INTRODUCTION

1.1 Background of Study

Every year, there is a gradual increase in accidents involving bone fractures. Bone fractures are a major orthopedic problem which most fractures are impossible to medicate externally as surgical bone implants are required. In the United States, about 1.3 million from 6.8 million medical attentions involved bone fracture surgical procedures each year (Levit, Wier, Stranges, Ryan, & Elixhauser, 2009; Zhang & Ma, 1999). Hence, implantation is no longer a rare medical procedure. Implant is a device artificially manufactured for medical purpose in such to replace, support or enhance biological structure that is missing, damaged or defected (Xu, Yu, Zhang, Pan, & Yang, 2007). Most of the short term implants are made from medical grade materials and non-biodegradable. The implant needs to be removed after the bones have healed. The implant needs to be removed after bones have healed in order to prevent local inflammation. This may cause morbidity rate of patient to increase as well as the cost of health care due to longer hospitalization (Fischer, Pröfrock, Hort, Willumeit, & Feyerabend, 2011). In recent years, magnesium alloys have gained a lot of interest for numerous applications such as aerospace, electronics, automotive part and biomedical. Their mechanical properties that is similar to natural bone, ability to degrade in chloride containing solution (Dorozhkin, 2014) and Mg also non-toxic to human body with 250 - 500 mg/day as an average daily dose for an adult (Hornberger, Virtanen, & Boccaccini, 2012; Song & Song, 2007). These properties have made them a potential biodegradable implant for short term application. Mg is the 11^{th} most abundant element in the body and plays significant role in biological system. Despite all of the promising aspects Mg has low surface stability which leads to rapid degradation. The degradation rate needs to be controlled in order it to coincide with the healing of the damaged bone.

Surface coating can decelerate the corrosion process. The coating layer should be in nanostructured form in providing more sites for ions absorption to enhance osteogenesis (Ma, Thompson, Zhao, & Zhu, 2014). Poly-L-lactic acid (PLLA) is synthetic copolymer that can easily formed nanostructured fibers with optimized parameter. It has interesting properties compared with other polymer. PLLA shows good adhesion properties. It takes longest time to be degraded but it shows faster response time compared to other polymer fibers. The homopolymer of L-lactide of PLLA has ability to strength the adhesion with surface of implants. It has been documented that PLLA degrades slowly and take more than 5 years to absorb (Bergsma et al., 1995; Kister, Cassanas, & Vert, 1998).

Electrospinning is the most versatile process in fabricating nanofibers. Electrospinning, which is also known as electrostatic spinning, is the most favorable process because of their simple set up and ability to form fibers from diversity of polymers with morphology and dimension suitable as growth substrates for various cells and tissues (Fang, Wang, & Lin, 2011).

In this research, HP Mg and AZ91 will be coated with nanofibrous PLLA by electrospinning to develop new potential biomaterial which not only cost effective but also safer for human.

.

1.2 Problem Statement

Magnesium and its alloys have been widely studied as implants due to its biodegradability which may eliminate removal procedure after bone is healed and properties similar to natural bone. However, its low corrosion resistance due to low surface stability, surface protection by polymer coating is necessary. Polymer coating is a cost-effective solution with potential to inhibit corrosion on Mg surface. However, it is still significant to determine the effect of polymer coating whether it can sufficiently control the degradation in physiological environment.

1.3 Objectives of Study

The objectives of this dissertation are listed as below:

1. To coat HP Mg and AZ91 with PLLA by electrospinning.

2. To study the corrosion behavior of coated and uncoated HP Mg and AZ91 in Hank's solution at body temperature (37 ºC) and pH 7.

1.4 Scope of Research

In the present study, HP Mg and AZ91 has been coated with PLLA using electrospinning method. The purpose of coating is to delay initiation of corrosion by HP Mg and AZ91. This research work investigates the corrosion rate of coated and uncoated HP Mg and AZ91 in Hank's solution.

The surface charaterization has been done to the HP Mg and AZ91 before and after coating with PLLA by using scanning electron microscope (SEM) coupled with energy dispersive X-ray spectroscopy (EDX). The physical and mechanical properties such as thickness and adhesion has been determined by surface profiler and microscratch test. The corrosion rate has been evaluated by hydrogen evolution volume and weight loss of HP Mg and AZ91 samples. The hydrogen evolve has been evaluated during immersion while the weight loss after immersion test in Hank's solution for 14 days. The surface characterization of HP Mg and AZ91 before and after corrosion product has been removed are identified by scanning electron microscope (SEM). This reseach reports on the ability of polymer coating to protect Mg surface from rapid corrosion.

1.5 Dissertation Overview

This dissertation is divided into five chapters. Chapter one states briefly the research background, problem statement, objectives of the study and scope of research. Chapter two presents the survey of existing literature on topics that related with this study. These topics include metal implants, surface modification technique, polymeric coating, coating techniques and magnesium corrosion. The research methodology is presented in chapter three which describes research flowchart, chemicals and reagent, preparation of magnesium specimens, preparation of PLLA coated Mg specimens by electrospinning, Mg and AZ91 characterization, immersion test and corrosion evaluation. Chapter four of this dissertation explains the results and discussion of the obtained findings. Chapter five states the conclusions of the study and recommends the possibilities for future works in this field.

CHAPTER 2: LITERATURE REVIEW

2.1 Metal Implants

A good implant must have the ability to degrade after the bone has healed. The surface of long term implant must well adhere to tissue cell and importantly, it must be offensive to bacteria to control infection (Chen, Gu, Lee, Lee, & Wang, 2012). Implants are divided into two types; traditional permanent implant and biodegradable implant. The examples of traditional implants are 316L stainless steel, pure titanium (Ti) and its alloy, and cobalt-chromium-based alloys. Traditional implants are well known for their ability in healing the damaged tissues. Unfortunately, if these implants remain in the human body for a longer period, toxic elements will be released to impair human body's health (Y. W. Song, Shan, & Han, 2008). This finding was agreed by other researcher. According to Abdal-hay, Barakat, & Lim (2013), the bone adhered to an implant will undergo a reduced load and eventually lose its density if the implant carries an enormous size of a component of the applied load. Stress shielding in bone is more harmful as a larger portion of the load is carried by the metallic implants. This stress shielding hinders the stabilization of the natural bone tissue. Therefore, multiple surgeries need to be performed, causing to additional complications.

The condition may worsen as long term unfavorable outcomes or effect from local inflammation possibly happen after a long period of implantation due to the metallic implant is a foreign object to human tissues. In addition, the removal surgery will only increase the morbidity rate of patients, cost of health care and hospitalization which not give any benefit to patients. A biodegradable implant will not cause permanent physical irritation or chronic inflammatory discomfort in comparison with the traditional permanent implant. This is because a biodegradable implant can be gradually dissolved, absorbed and consumed by human tissue. Thus, there is no need for another surgery to

remove the implants after the wound has healed (Wen et al., 2009). At present, biodegradable implants are made of polymer (W.-J. Li, Cooper, Mauck, & Tuan, 2006).

There are many types of metals and alloys are usually used to make an implant for medical purposes. The most popular are 316L stainless steel, titanium alloys and cobalt based alloys. Each of them has their own special character to be used as implant (Jacobs, Gilbert, & Urban, 1998). According to Ostrowski et al. (2013), the implementation of stainless steel or titanium as biomedical implants is favourable for medical application that requires load-bearing capacities. Besides that, a typical 316L stainless steel is stronger and cheaper while cobalt alloys exhibit reasonable biodegradation properties when exposed to human tissues. However, these metals also have their weaknesses. Stainless steel is easily corroded. Titanium can deteriorate, dissolve and expose the metal to corrosion (Bajgai et al., 2011). For the past few years, titanium is gaining a lot of attention as it has been widely used in multiple applications such as food coloring, paints, cosmetics, catalysts, anti-bio fouling and others. Furthermore, titanium has also received popularity in photonic band gap crystals for visible spectrum of light due to its suitable energy band gap (≈ 3.2 -3.5 electron volts, eV), high refractive index (n rutile ≈ 2.9) and low absorption characteristic. Lately, it is also reported that titanium dioxide (TiO_2) coats self-cleaning wool-polyamide, polyester and cotton textiles. Recently, Ti and its alloys are the main material in medical application especially for hard tissue replacement, such as orthopaedic and cardiovascular synthetics. This is due to its biological safety, high corrosion resistant, superior bio-compatibility and excellent mechanical strength (Iafisco, Foltran, Sabbatini, Tosi, & Roveri, 2011).

However, when it is subjected to severe mechanical loading, TiO_2 film can deteriorate and dissolve, expose the unprotected metal to corrosion (Abdalla, Hwang, & Lim, 2012). Moreover, like some other metal, titanium also exhibit poor bioactive properties.

In general, human tissues will react with the outermost layers of the implant. Therefore, surface layer plays a very important part in the immediate reaction. However, due to the titanium nature inertness, titanium implant has difficulties to achieve good chemical bonding limiting its direct bonding with the local tissue to promote osseointegration (Castellani et al., 2011).

2.1.1 Magnesium and Its Alloys for Implants

Magnesium (Mg) gained numerous interests in many fields such as aerospace, automotive, electronics and biomedical. Superior properties of Mg alloys such as their low density, high specific strength, good castability, comparable corrosion rates in physiological media and excellent electromagnetic shielding make them favorably to be used as implant especially in cardiovascular interventions and osteosynthesis (Abdal-hay, Dewidar, Lim, & Lim, 2014).

Furthermore, Mg is biodegradable, environmentally friendly and crucial to human metabolism and exists in bone tissue (Porter, Kaplan, Homeier, & Beers, 1995). According to Wen et al (2009), Mg is to be considered an ideal biodegradable implant because of its low density, high strength to weight ratio; specific elastic modulus and specific yield strength closer to the bone tissue than the conventional implants. Mg alloys could decrease the stress shielding since the modulus of elasticity is closer to the bone (Chou et al., 2013). Moreover, Mg and its alloy fulfilled the loss of bone density (Zhao et al., 2017). The summary of the physical and mechanical properties of various implant materials in comparison to natural bone is shown in Table 2.1(Staiger, Pietak, Huadmai, & Dias, 2006).

Secondly, Mg and its alloy are non-toxic to the human body below its tolerates level limit of 250 - 500 mg/day for an adult (Witte, 2015). Mg deficiency can accelerate the

risk of hypertension, cardiac arrhythmias and osteoporosis (G. Song, 2007). It is found that the deposition of Mg ion is harmless to human body and it also can enhance the growth of new bone tissue (Zreiqat et al., 2002). Lastly, Mg is biodegradable in body fluids since Mg alloy can dissolve slowly, adsorb and excrete after implantation. As a proof, Mg alloys could decrease the stress shielding since the modulus of elasticity is closer to the bone (Chou et al., 2013). Moreover, Mg and its alloy fulfilled the loss of bone density. As a result to this, biodegradable Mg implant omit the removal procedure that is needed for second surgical intervention (Zhao et al., 2017).

However, Mg and its alloys have their weakness. In a solution containing chlorides such as human body fluids or blood plasma, Mg and its alloys suffered an attack due to its weak surface stability resulting them to corrode quickly (Chaya et al., 2015). High purity Mg alloys (with impurities concentration below their tolerance limits) will have corrosion rates extremely lower than low purity alloys (Cao, Shi, Song, Liu, & Atrens, 2013). Besides that, the formation of unwanted possibly harmful hydrogen gas pockets under the skin may lead to the failure of a surgery before the healing process start. The gas pockets formation can be stopped by controlling the degradation of Mg alloys (Wong et al., 2010). Furthermore, if a Mg alloy implant is used to repair bone tissue diseases, it may lose its mechanical strength before the healing of bone tissue due to high corrosion rate (Abdal-hay, Dewidar, & Lim, 2012). This result agrees with the previous study that the mechanical integrity of the Mg-Cd to secure fractures were only maintained for 6-8 weeks. This is due to the release of hydrogen during corrosion process.

The weak corrosion resistance of Mg biodegradable implant needs to be improved by having appropriate alloys compositions, as well as by applying surface treatments such as coating (Troitskii & Tsitrin, 1944). Besides that, Mg implants do not directly bond with local bone tissue or promote osteogenesis. If only implants are positioned correctly

and infection is evaded, it is believe that they will sustain for a long period. Geometry and surface topography are vital for the short-term and long-term success of the implant. Therefore, surface modification is important to improve the osseointegration and biological function of implants.

Table 2.1: The physical and mechanical properties of different type of implant materials in comparison to natural bone.

Properties	**Natural bone**	**Mg**	**Ti alloy**	**Co–Cr alloy**	**Stainless steel**	**Synthetic hydroxyapatite**
Density (g/cm3)	1.8–2.1	1.74–2.0	4.4–4.5	8.3–9.2	7.9–8.1	3.1
Elastic modulus (Gpa)	3–20	41–45	110–117	230	189–205	73–117
Compressive yield strength (Mpa)	130–180	65–100	758–1117	450–1000	170–310	600
Fracture toughness (MPam1/2)	3–6	15–40	55–115	N/A	50–200	0.7

2.2 Surface Modification Techniques

The main factor that influences cellular interactions and tissue integration of the implant site is the surface properties such as morphology, roughness, and chemistry. Therefore, surface properties play an important role in determining implant material's biocompatibility, bioactivity and osseointegration. This is to improve the osseointegration and biological function of an implant. Over the last decade, a lot of efforts have been attempted to develop biodegradable and biocompatible scaffolds that are made from natural and synthetic polymer. Principally, the scaffold's design should mimic the structure and biological function of native extracellular matrix (ECM) proteins. The ECM consists of nanostructured to microstructured fibers. ECM is responsible to provide mechanical support and regulate cell activities (Rahmany & Van Dyke, 2013).

Many researchers have investigated the capability of fabricating bio-threads containing live cells in favorable polymeric matrices that are preferred for various applications such as wound healing and tissue growth. Electrospun fibers are discovered to have properties that bear morphologic similarity to the ECM of natural tissue such as high porosity and effective mechanical properties. This finding matches the important design aspect of a perfect engineered scaffold (Azad, McKelvey, & Al-Firdaus, 2008). Furthermore, electrospun fibers have high area-to-volume ratio and controllable porosity. The matrix texture, as well as the nature of the biomaterial, is crucial as it was also reported to control cell adhesion, proliferation, shape, and function (Byung-Moo Min, Young You, Jin-Man Kim, Seung Jin Lee, & Won Ho Park, 2004).

Coatings on the surface of implants are to increase corrosion resistance, antimicrobial action, dielectric strength and others. They are inexpensive to apply and environmental friendly (Chronakis, 2005). Recent studies concerning bio-based polymer coatings on

implants have revealed their excellent role in stimulating cellular responses to increase bone remodeling, bone growth and bone implant contact (Abdalla et al., 2012). One of the major causing the orthopaedic implant to fail is infection. Thus, infection control becomes particularly crucial and remains a long-standing challenge on abiotic surfaces. In preventing bacterial colonization, a continuous effort has been made to modify material surfaces. Tissue-integration with implant surface is not required for those short term implantation but it becomes highly required for long-term fracture fixation (Chen et al., 2012).

However, several concerns have been raised about the practice of coating porous Mg implants with bioactive material. These concerns include the limitation of space available for bone in-growth, challenging in coating biomaterials onto the uneven surface of implants and very low degradation rates of common coating materials (Guo, Glavas, & Albertsson, 2013). One of the ways is to make the materials to nanometer size. This will improve their properties and create new excellent properties that are better than the bulk properties. The superior properties of polymeric nanofibers such as the large surface area to volume ratio, flexibility in surface functionalities, and excellent mechanical performance, have made it fabricated for numerous uses, such as in drug delivery, tissue engineering and wound healing (Chu, Chen, Wang, & Huang, 2002). However, resulting from the decreased grain size and diameter of surface pores, the nanostructured surfaces of nanomaterials possessed greater surface roughness. Hence, leads to enhancement of surface wettability compared to the conventional surfaces.

2.3 Polymeric Coating

Polymers that are used as coating are divided into several types such as natural polymer and synthetic polymer (Liang, Hsiao, & Chu, 2007; Hai-Sheng Wang, Guo-Dong Fu, & Xin-Song Li, 2009). Polymeric coating has been used to control the rate of Mg degradation and to produce good biocompatibility and biostability, thromboresistance, antimicrobial action, dielectric strength, wear properties and lubricity. Therefore, it may make the application of medical implant in human body more practicable and favorable. In addition, polymer coating is inexpensive to apply and environmentally friendly. Conversion coating is a general type of metal-based implants coating. The conversion coating is formed in situ, through a reaction between the metal substrate and its environment, and it's typically inorganic (Abdal-hay, Barakat, & Lim, 2013). Table 2.2 shows the properties of different polymers used in medical application (Hai-Sheng Wang, Guo-Dong Fu, & Xin-Song Li, 2009). The properties and degradation rate of synthetic polymeric nanofibers such as poly(ε-caprolactone) (PCL), poly(L-lactic acid) (PLLA), poly(glycolic acid) (PGA) and poly(lactic-co-glycolic acid) (PLGA), and naturally-occurring polymeric nanofibers such as collagen are shown in Table 2.3 (Ravichandran, 2009).

Table 2.2: Type of polymers and their properties.

Type of polymer	Properties
Natural Polymer	• Low toxicity and exhibits better biocompatibility • Good physicochemical properties • Required complicated solvents to be used with electrospinning process such as hexafluoroisopropyl alcohol and formic acid • Examples: Collagen, gelatin, and silk fibroin
Synthetic Homopolymers	• Biocompatible and biodegradable • Easy to form through electrospinning process but the fiber surface structure is hard to be optimized • Solvent used for electrospinning process in industrial production can be classified as poisonous when it evaporated • Example: Poly (vinyl alcohol) (PVA), polycaprolactone (PCL) and polylactide (PLA)

Table 2.2 (continued)

Synthetic Copolymers	• Modified new functional fiber materials with advanced properties such as electrospun fibers of block copolymers are produced • Electrospun fiber mat with better properties is produced • The response time of electrospun fiber is faster than the film due to larger external surface area • The fibers have mixture of different mechanical properties compared with homopolymer • Examples: Poly (lactic-co-glycolic acid) (PLGA) and poly (L-lactic acid) (PLLA)

Table 2.3: The properties and degradation rates of nanofibers polymers.

Polymer	Properties	Degradation rate (month)
Poly(glycolic acid) (PGA)	Aliphatic polyester, Crystalline, semi permeable	6-12
Poly(L-lactic acid) (PLLA)	Aliphatic polyester, crystalline, porous; Rough-looking due to the open-pore structure	>24
Poly(lactic-co-glycolic acid) (PLGA)	Semi permeable	6-12
Poly(ε-caprolactone) (PCL)	Semi permeable, amorphous	<12
Collagen	Semi permeable	1-9

2.3.1 Poly (L-lactic) Acid (PLLA)

In recent years, research in polymers have received great attention because of their applications in surgical and biomedical. Figure 2.1 illustrated the chemical structure of PLLA bonding on Mg surface. Usually, organic coatings are linked to metals by hydrogen bonding. PLLA is acronym used to represent homopolymer and stereocopolymer of lactic acid. One of the properties of PLLA is known as aliphatic polyesters. Aliphatic polyesters are derived from lactidestereomers (LA) which considered as renewable resources (Gupta, Revagade, & Hilborn, 2007). Aliphatic polyesters have significant interest in medical application such as in tissue fixation (i.e., bone screws, bone plates, and pins), drug delivery systems (i.e diffusion control), wound dressing (i.e artificial skin) and wound closure (i.e sutures and surgical staples) (Tian, Tang, Zhuang, Chen, & Jing, 2012). Medical devices made from polylactic acid (PLA) such as bone screws, bone plates and pin structures are being used and forecasted to replace metal implants later (G. Kister, G. Cassanas, & M. Vert, 1998; Pandey, Pandey, & Aswath, 2008). PLLA has good mechanical properties compared to other polymers. The degradation rate usually depends on the biological and physical properties of PLLA on Mg surface (Lim, Auras, & Rubino, 2008). One major advantage of PLLA is it is hydrophobic and having low contact angle. Thus, compared to other polymers, PLLA has longer degradation duration. Moreover, it also has good biocompatibility and biodegradable. The usage of PLLA in biomedical application started in the early 1960s until nowadays. PLLA has been approved by the U.S. Food and Drug Administration (FDA) as biodegradable polymer and it is commercially available in various grades (Zhang & Ma, 1999). These biodegradable polymers have several advantages such as no removal surgery required and no stress-shielding effect. It is reported that degradation of PLLA is non-acidic. It induces deposition of calcium phosphate compound in vivo thus lead to no metallic corrosion (Krikorian & J. Pochan,

2003; Byung-Moo Min, Young You, Jin-Man Kim, Seung Jin Lee, & Won Ho Park, 2004). PLLA also has good adhesion properties. Corrosion protection depends on adhesion bonding between the coating and metal substrate (Armentano, Dottori, Fortunati, Mattioli, & Kenny, 2010).

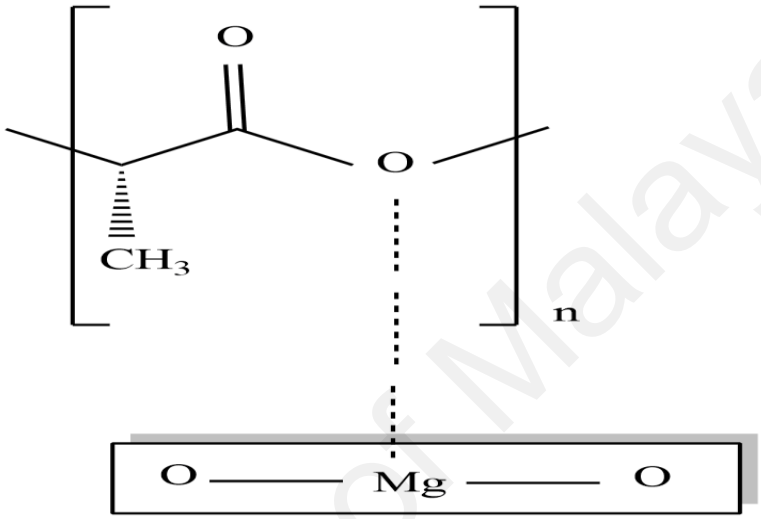

Figure 2.1: Chemical structure of poly (L-lactic acid) (PLLA) on Mg.

2.4 Coating Techniques

The biodegradable coating implant for tissue engineering can be manufactured by various processes like electrospinning, phase separation, self–assembly and lithography. Comparisons between the various techniques are shown in Table 2.4 (Dorozhkin, 2014).

Table 2.4: Various coating techniques along with their advantages and disadvantages.

Coating technique	Advantage	Drawback
Laser deposition	• Simple and fast technique with uniform distribution of pore size	• End product has poor surface finish • Reduced its resolution
Self assembly	• Its spontaneous assembly eliminates cell-seeding instead prefabricated scaffold is used • Fibrous networks are produced to support cells in 3D	• Lack of mechanical strength • Produces short and random nanofibers with limited amphiphilic property
Lithography	• Relatively good resolution	• Time consuming • Expensive
Electrospinning	• Capable of mimicking the stem cell niche by manipulating the spinning parameter such as the diameter of fiber	• Cell infiltration problems yields a flat mat that has limited 3D due to the small pore size of the fibers
Phase separation	• Has desirable high porosity and surface-to-volume ratios that are suitable to produce nanofibrous scaffold	• Nanofiber distribution is subjected to the the processing method used

2.4.1 Electrospinning Process

Among many techniques of fabricating nanofibers, electrospinning is perhaps the most preferable process. Electrospinning is well known for its simple fabrication setup and the ability to produce fibers from a different type of polymers, and significantly, their morphological and dimensional similarity to native extracellular matrix (ECM). Subsequently making electrospun fiber meshes gained a lot of interest to be used as growth substrates for various cells and tissues (Khajavi & Abbasipour, 2012; Shah, Manthe, Lopina, & Yun, 2009). This process is preferred to produce nanofibrous structures from natural and synthetic polymers such as collagen, silk fibroin, poly(lactide), polycaprolactone, and others (Croisier & Jérôme, 2013; Iafisco et al., 2011).

In the electrospinning, the polymer solution at the end of a capillary tube is held by its surface tension which is subjected to an electric field. The charge is induced by an electric field on the liquid surface. A force directly opposite to the surface tension is developed due to the mutual charge repulsion. The hemispherical surface of the solution at the tip of the capillary tube elongates to form a conical shape known as the Taylor cone as the intensity of the electric field is higher (Duan et al., 2007). A charged jet of the solution is ejected from the tip of the Taylor cone, when the electric field reaches a critical value at which the repulsive electric force overcomes the surface tension force. Its trajectory can be controlled by an electric field. The solvent evaporates when the jet travels in the air, leaving behind a charged polymer fiber which forms itself randomly on the metal collector. Thus, a non-woven fabric formed by continuous fibers being laid (Doshi & Reneker, 1995).

Electrospinning had known as an excellent nano manufacturing process in tissue engineering. Electrospinning process is popular in both academic research and industry

because it can produce high yielding nanofiber at low cost compared to other processes such as phase separation, laser deposition and others (Frenot & Chronakis, 2003).

In order to get uniform fibers with three-dimensional pore structure with high porosity and appropriate for self-assembling mineralization, there are several parameters need to be optimized. These parameters are viscosity, conductivity, and surface tension; controlled variables including hydrostatic pressure in the capillary, electric potential at the tip, and the distance between the tip and the collection screen; and ambient parameters including temperature, humidity, and air velocity in the electrospinning chamber. Factors that can affect the electrospinning process and fiber morphology are shown in Table 2.5 (Sun et al., 2014).

Table 2.5: Factors affecting the electrospinning process and fiber morphology.

Parameter	Effect
Conductivity	• Higher conductivity tends to yield smaller fibers with uniform bead-free and decrease fiber diameter
Viscosity/concentration	• High concentration or viscosity will increase fiber diameters
Polymer molecular weight	• High polymer molecular weight will decrease the number of beads and droplets
Dipole moment and dielectric constant	• Successful spinning occurred in solvents with a constant high dielectric
Flow rate	• Low flow rates will reduce fiber diameter • High flow rates increase fibers yielding that are not completely dried on the collector
Field strength/voltage	• Large fiber diameter is produced at extreme high voltage
Distance between tip and collector	• Fiber diameter decreases with the increment of distance • Beading is observed at close and far distance hence distance optimization is required
Fiber morphology	• Metal collectors collect smooth fibers.
Ambient parameters	• Solution viscosity is decreased at high temperature resulting smaller fibers • Pores appeared on the fibers at high humidity

In general, electrospinning is a simple, versatile, cost-effective and scalable system that uses a high voltage electrical field to generate aligned or random nanofibers from several synthetic and natural polymers.

2.5 Magnesium Corrosion

Mg and its alloys are popular and gaining interest to be considered as implant material due to their properties. Mg not only has an elastic modulus close to the bone but also has a great combination of load bearing mechanical characteristics and restrainable corrosion rates (Witte et al., 2008; Zainal Abidin et al., 2013).

The overall corrosion reaction of magnesium in aqueous environments is given as follows (Atrens, Liu, & Abidin, 2011):

$$Mg_{(S)} + 2\,H_2O_{(aq)} \rightleftharpoons Mg(OH)_{2(s)} + H_{2(g)} \quad (2.1)$$

This overall reaction may include the following partial reactions:

$$Mg_{(S)} \rightleftharpoons Mg^{2+} + 2e^- \text{ (anodic reaction)} \quad (2.2)$$

$$2H_2O_{(aq)} + 2e^- \rightleftharpoons H_{2(g)} + 2OH^- \text{ (cathodic reaction)} \quad (2.3)$$

$$Mg^{2+} + 2OH^- \rightleftharpoons Mg(OH)_{2(S)} \text{ (product formation)} \quad (2.4)$$

Mg alloys function as an anode where Mg dissolution reaction is combined with cathodic water decomposition which then evolved H_2 gas by a direct reduction from water, H_2O (Virtanen, 2011). The corrosion of Mg converts metallic Mg to the stable ion, Mg^{2+} given by Eq. (2.2). These anodic partial reactions are balanced by the cathodic partial reaction of hydrogen evolution (Eq.(2.3)). In the absence of aggressive anions such as chloride ion, protective and stable magnesium oxide can be produced on

the surface. For every Mg atom dissolved, one hydrogen molecule is evolved which the corrosion rate of Mg can be measured by measuring the evolved hydrogen rate (Zainal Abidin, Martin, & Atrens, 2011).

However, Mg alloys susceptibility to high corrosion rate hinders its clinical applications. This is due to poor corrosion resistance which leads to high driving force for corrosion making it an active metal. The second phase causes the acceleration of the micro-galvanic corrosion. Its means Mg alloys corrode faster than HP Mg (Qiao, Shi, Hort, Zainal Abidin, & Atrens, 2012; Zainal Abidin et al., 2013).

In studying the corrosion of Mg alloys, HP Mg was used as a standard. HP Mg means that the impurity elements (Fe, Ni, Cu and Co) are each below their (alloy dependent) tolerance limit. The corrosion rate is greatly increased when the content of the impurity exceeds the tolerance limit, whereas, the corrosion rate is low when the impurity content is lower than the tolerance limit. The impurity elements (Fe, Ni, Cu and Co) were playing an important role which they can greatly affect the Mg binary alloys in salt-water environment. These impurity elements have extremely harmful effects because of their low solid-solubility limits in alpha-Mg (α-Mg) and their capabilities to react as active cathodic sites (Atrens, Liu, & Zainal Abidin, 2011).

Other parameters that influence the corrosion rate are the pH and media of solution. Even in a neutral bulk solution, the pH might increases until the precipitation of $Mg(OH)_2$ is achieved forming a partially protective layer at pH of 10.5. The release of gaseous CO_2 also causing the pH to increase. This might be attributed to the equilibrium of CO_2 and the bicarbonate ions. This equilibration reaction can be overcome by a CO_2 gas supply into the solutions (Zainal Abidin et al., 2011). Calculations showed that an increase in pH leads to a strong supersaturation. Chloride ions promote rapid attack in neutral solution and even more so in acidic solutions. In alkaline or poorly buffered

chloride solutions, the pH can increase due to formation of a partially protective $Mg(OH)_2$ layer, which is very stable at pH 11.5 hence, lowering the corrosion rate of Mg alloys (Dhanapal, Boopathy, & Balasubramanian, 2012; Jönsson, Persson, & Thierry, 2007; Y. Li, Lee, Cui, & Choi, 2008).

CHAPTER 3: RESEARCH METHODOLOGY

3.1 Research Flowchart

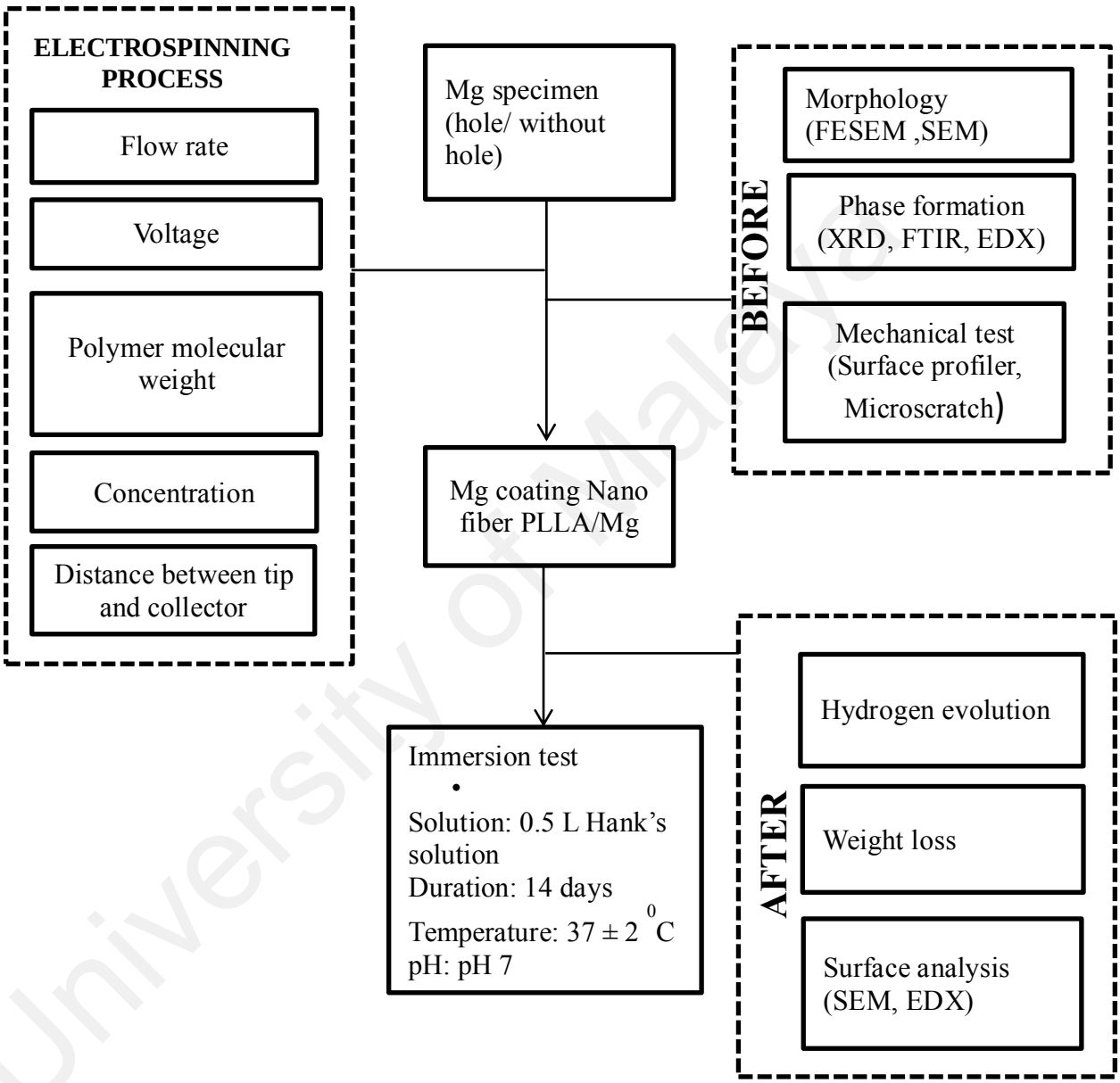

Figure 3.1: Single step of work scope.

3.2 Chemicals and Reagent

All used chemicals (Chloroform and Hank's balanced salt) were analytically grade and purchased from Systerm and Sigma Aldrich respectively. Table 3.1 presents the elements compositions of HP Mg and AZ91 by X-ray fluorescence (XRF). Table 3.2 shows chemical composition of Hank's solution compared with simulated body fluids and the inorganic human blood plasma.

Table 3.1 Elements content, wt% of HP Mg and AZ91.

Element	HP Mg (wt%)	AZ91(wt%)
Mg	Balance	Balance
Al	0.0088	8.15
Zn	0.02	0.64
Mn	0.02	0.15
Cu	<0.01	<0.01
Fe	<0.01	<0.01
Ni	<0.01	<0.01
Ca	<0.005	<0.01
Be	<0.0001	<0.0001
Ce	<0.01	<0.01
Gd	<0.01	<0.01
La	<0.01	<0.01
Nd	<0.01	<0.01
Pr	<0.01	<0.01
Y	<0.01	<0.01

Table 3.2 Chemical composition of Hank's solution compared with simulated body fluids and the inorganic human blood plasma.

Solution	Composition (mmol L^{-1})									
	Na^+	K^+	Mg^{2+}	Ca^{2+}	Cl^-	HCO_{3-}	$H_2PO_4^-$	HPO_4^{2-}	SO_4^{2-}	OH^-
Hank's	142	5.8	0.8	2.5	145	4.2	0.4	0.3	0.8	-
SBF5	142	5.0	1.0	2.5	131	5.0	-	1	1.0	
SBF27	142	5.0	1.0	2.5	109	27	-	1	1.0	
Blood plasma	142	3.6-5.5	1.0	2.1-2.6	95-107	27	-	0.7-1.5	1.0	-

3.3 Preparation of Magnesium Specimens

Samples with dimensions of (10 x 10 x 5 mm) were cut from high purity magnesium (HP Mg) and AZ91 ingots (purchased from China) respectively. All sample surfaces were mechanically polished with 1000-1200 grit silicon carbide (SiC) papers and cleaned with ethanol and distilled water. There were four types of samples; HP Mg, AZ91, PLLA-HP Mg and PLLA-AZ91. Sixtuplicate samples were prepared for each type. Three samples from each type were drilled with hole in the middle of the square shaped samples having diameter of 1.0 mm to mimic the sample for in vivo. Three samples without hole were also prepared to obtain uniform coated surface for immersion test. Separated samples were prepared for coating characterization purpose. Samples dimension is shown in the Figure 3.2 below. Table 3.3 presents type of sample used.

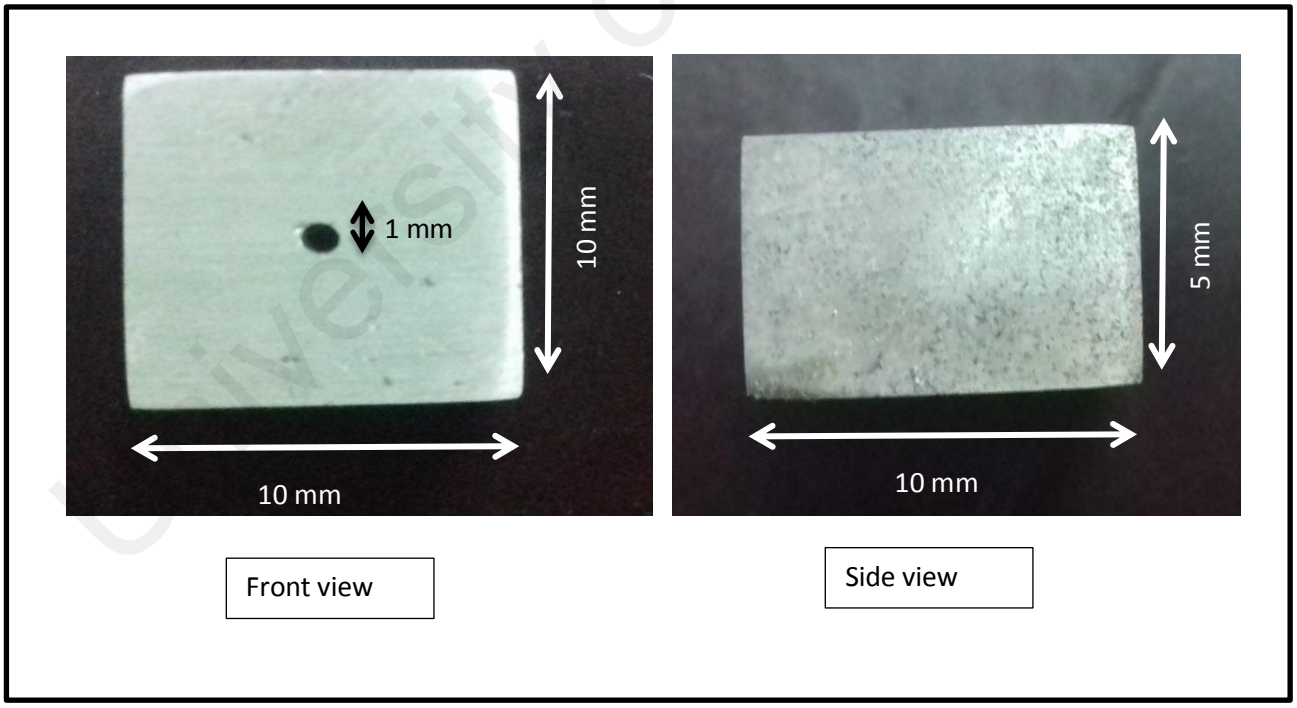

Figure 3.2: Prepared sample.

Table 3.3 Types of sample.

Types of sample	Mg sample	Sample No.
hole	HP Mg	HP Mg 1
		HP Mg 2
		HP Mg 3
	AZ91	AZ91 1
		AZ91 2
		AZ91 3
	PLLA-HP Mg	PLLA-HP Mg 1
		PLLA-HP Mg 2
		PLLA-HP Mg 3
	PLLA-AZ91	PLLA-AZ91 1
		PLLA-AZ91 2
		PLLA-AZ91 3
without hole	HP Mg	HP Mg 4
		HP Mg 5
		HP Mg 6
	AZ91	AZ91 4
		AZ91 5
		AZ91 6
	PLLA-HP Mg	PLLA-HP Mg 4
		PLLA-HP Mg 5
		PLLA-HP Mg 6
	PLLA-AZ91	PLLA-AZ91 4
		PLLA-AZ91 5
		PLLA-AZ91 6

3.4 Preparation of PLLA Coated Mg Specimens by Electrospinning

The electrospinning apparatus consists of three components: (i) spinneret, (ii) collector, and (iii) high voltage power. PLLA solution was prepared by dissolving 8 wt% PLLA (Mitsui Chem. Co. Ltd. The weight-average molecular weight of PLLA was 1.63 x 10^5 $g.mol^{-1}$) in chloroform by magnetic stirring at room temperature. The solution was fed into a 10 ml syringe with thin needle (27 G; inner diameter (ID) 0.21 mm and outer diameter (OD) 0.42 mm) which was installed on a syringe pump and a PLLA dope was extruded from the syringe at a constant rate. The parameters for electrospinning were as follows: applied voltage 10 kV, distance tip to collector 15 cm and feed rate 1 ml/hr (Amalina, Hajime, Hideki, Yoshiharu, & Shigeyuki, 2009). Figure 3.3 shows the schematic diagram of electrospinning set-up.

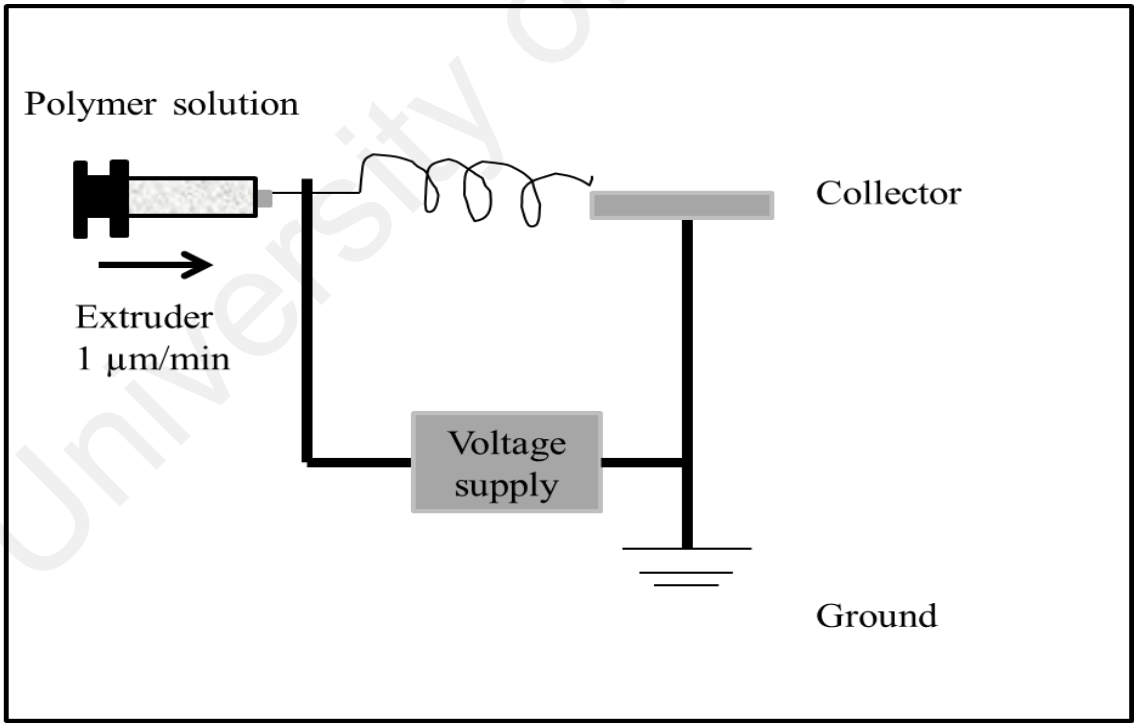

Figure 3.3: Schematic diagram of electrospinning set-up.

3.5 Mg and AZ91 Characterization

3.5.1 PLLA-Mg Formation

The surface morphology of the Mg samples before and after immersion test was characterized by scanning electron microscope coupled with an energy dispersive X-ray spectroscopy (EDX), X-Ray Diffraction (XRD) and Fourier Transform Infrared Spectrometer (FTIR).

3.5.1.1 Scanning Electron Microscope (SEM/ SEM-EDX)

All SEM analyses were performed using Phenom SEM Table Top system. The instrument was used to observe the surface morphology of Mg before and after immersion test. The observation was done in an accelerating voltage of 10kV and 15kV. The magnitude was varied from 500x to 1500x. Typical images for surface before and after immersion test were selected through SEM observation for further analysis. The analysis to identify compound that deposited on surface of Mg before and after immersion test was performed by Phenom, energy dispersive X-ray spectroscopy (EDX).

3.5.1.2 X-Ray Diffraction (XRD)

In this research, XRD was employed using CuKα radiation, with wavelength was approximately 1.54 Å at 45 kV and 40 mA. XRD was used to identify the phase of the material and the type of compounds present. XRD was applied on the Mg samples before and after coated with PLLA to prove the existent of PLLA on top of Mg surface.

3.5.1.3 Fourier Transform Infrared Spectrometer (FTIR)

All FTIR analyses were performed by Perkin Elmer model. Fourier Transform Infrared analysis was applied on the PLLA coated on Mg before and after immersion test to determine functional groups (corrosion product) formed on the surface of Mg and in Hanks' Solution. The spectra were recorded from 4000 to 400 cm^{-1}.

3.5.2 Determination of Mg Coating Effectiveness

The cross-section of the sample was observed using field-emission scanning electron microscopy (FESEM) to better reveal the coating and thickness. The formation of polymer (PLLA) layer on Mg surface was identified using Fourier transform infrared spectrometer (FTIR) in the range of 4000-400 cm^{-1}. The thickness and adhesion strength between PLLA layer and Mg was determined by microscratch test. The standard test of ASTM 3359 was done to qualify the adhesion strength of PLLA layer on Mg surface. The thickness test was determined by Surface profiler to confirm the thickness of PLLA layer.

3.5.2.1 Field-Emission Scanning Electron Microscopy (FESEM)

FESEM were used to identify the thickness of PLLA coating on Mg surface. The Mg samples were prepared by cold mounting in Poly-vinyl alcohol (PVA) solution. PVA solution acts as hardener to provide the mounting compound. Cold mounting compound were preferred for PLLA-Mg sample that is sensitive to the heat or pressure, which applied in hot mounting. After mounting, sample surface were grind and mechanically polished with 1000-1200 grit silicon carbide (SiC) papers before captured by FESEM. The instrument also used to determine surface morphology of Mg after immersion test was done, and before corrosion product removal. A thin layer of platinum and aurum

were covered the sample using sputter coater before observation. The observation is prepared in an accelerating voltage of 15kV.

3.6 Immersion Tests

The immersion test was done to study the corrosion resistance of the coated and uncoated high purity magnesium (HP Mg) and AZ91 (Zainal Abidin, Atrens, Martin, & Atrens, 2011). This test was done by hanging the specimens with fishing line as shown in Figure 3.4. Each sample was immersed for 14 days at 37 ± 2 ^{0}C in 0.5 L Hank's solution. To prepare Hank's solution, 9.7 g of Hank's balanced salt (without sodium bicarbonate and phenol red, Sigma Aldrich) was mixed with 0.35 g of sodium bicarbonate (reagent grade) in 1 L of distilled water. By bubbling CO_2 at a partial pressure of 0.009 atm during the immersion test, the solution pH was maintained constant at pH 7.

The corrosion rate was determined by (i) the hydrogen evolution volume and (ii) the weight loss during the entire period of immersion test.

The overall Mg corrosion reaction is given by:

$$Mg + 2\,H_2O \rightarrow Mg^{2+} + 2OH^- + H_2 \qquad (3.1)$$

Eq. (3.1) shows that each atom of corroded Mg comes along with the evolution of one molecule of hydrogen. Hydrogen evolution was collected directly by a filter funnel into burette above corroding sample. After immersion test was done, the sample is taking out from the solution and dries in the desiccators for 1-2 days.

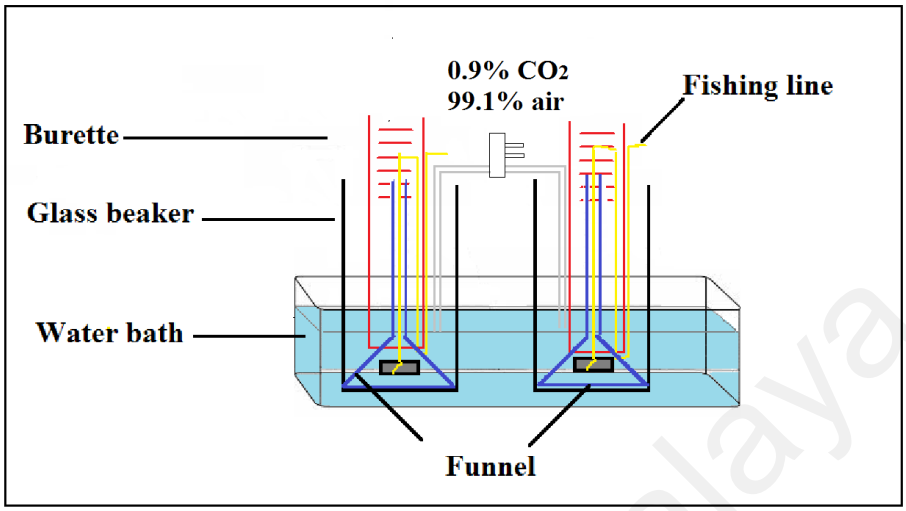

Figure 3.4: Schematic diagram for an immersion test of specimen hung with fishing line.

3.7 Corrosion Evaluation

In order to evaluate the corrosion rate P_{AH} (mm y^{-1}) using a compatible gas law to the standard temperature (0°C) and pressure (1 atm) were converted during the immersion test with the amount of hydrogen volume (V_H) that have been collected along the process.

$$P_{AH} = 2.279\, V_H \tag{3.2}$$

The corrosion products were cleaned by putting of each sample in chromic acid cleaning solution at room temperature for 10 min. This chromic acid cleaning solution contained 200 g L^{-1} CrO_2 and 10 g L^{-1} $AgNO_2$.

After cleaning, each of the specimens was rinsed with distilled water. The specimen was then dried in desiccators for 1-2 days. The weight loss rate, W_L (mg cm^{-2} day^{-1}) as to be evaluated by using:

$$W_L = (Wb - Wa)/\, At \tag{3.3}$$

Where Wb (mg) represents the weight of specimen before immersion test, Wa (mg) was the weight after removal of corrosion product after immersion test was done, A represents the surface area of sample (cm^2) and t was the duration of immersion test in days (d). The weight loss was converted to the (average) corrosion rate, Pw (mm y^{-1}) (Shi & Atrens, 2011; Zhao, Liu, Song, & Atrens, 2008; Zhao et al., 2009):

$$Pw = 3.65\Delta\, W/\rho \tag{3.4}$$

Where $\Delta\, W$ represents the weight loss and ρ represents the metal density (g/cm^3). The density of Mg is 1.74 g/cm^3, thus:

$$Pw = 2.1\Delta\, W \tag{3.5}$$

While the surface of the Mg samples after immersion test were characterized by a scanning electron microscope (SEM) coupled with an energy dispersive X-ray spectroscopy and FTIR.

CHAPTER 4: RESULTS AND DISCUSSION

4.1 Sample Characterization

4.1.1 Physico-chemical Properties of HP Mg and AZ91

Figure 4.1 and Figure 4.2 shows the surface of HP Mg and AZ91. The microstructure of Mg after etching was observed on SEM photo and EDX spectra to determine the proportion of HP Mg and AZ91. Figures also represents the microstructure of HP Mg and AZ91 alloys as revealed using optical microscope after polishing with silica paper, cleaned with ethanol and distilled water then etching process was done on the specimen surfaces. Etching process helps to determine the α-phase which also known as micro-pores and it appeared as a dark region (J. Chen, Song, Shan, & Han, 2015). After polishing using SiC paper, the samples were etched using 3% natal. The grain size of all specimens was large, similar with their original state from cast mold. HP Mg has single phase, with pore along the limit and some pores inside the grain. AZ91 had two phases; α-Mg matrix and β-phase ($Mg_{17}Al_{12}$) particles. The results were similar with previous finding that the HP Mg surface is very compact, homogeneous and without excrescence due to single phase. Two phase microstructure of AZ91 caused by the hardness between the α-phase and β-phase by region that high content of Al (Elias, Oshida, Lima, & Muller, 2008; Yu et al., 2012; M.-C. Zhao, Liu, Song, & Atrens, 2008).

While the broad peak at 2Θ angle of 16º was found on the surface of both samples belongs to the diffraction peak of PLLA-HP Mg and PLLA-AZ91. This finding was reported by previous research where the diffractions of PLLA were not sharp (Amalina, Hajime, Hideki, Yoshiharu, & Shigeyuki, 2009; Krikorian & J. Pochan, 2003). This observation proved that PLLA layer was successfully deposited on Mg and AZ91.

4.2.2 Fourier Transform Infrared Spectrometer (FTIR).

FTIR were used to verify chemical structure of PLLA that were formed on HP Mg and AZ91 samples (Pandey, Pandey, & Aswath, 2008; Q. Zhang et al., 2012). Figure 4.4 and 4.5 represents the FTIR spectra of the surface of PLLA-HP Mg and PLLA-AZ91. The summary of functional group identified by FTIR was shown in Table 4.1.

Table 4.1: Functional group formed on samples surface.

Peaks (cm^{-1})	Functional group
2997	CH
2946	CH
1759	C=O
1456	CH3
1382	CH
1225	ester group
1090	C-O-C
945	PLLA

Both figures show same pattern of FTIR spectrum. The FTIR results are in good agreement with the previous study (Abidin, Martin, & Atrens, 2011; Zuwei Ma, Mao, & Gao, 2007).The transmittance peaks at 2997 cm^{-1} and 2946 cm^{-1} are attributed to the region of CH stretching. The C=O stretching region appeared at 1759 cm^{-1}. Transmittance peak at 1456 cm^{-1} and at 1382 cm^{-1} were assigned to CH_3 and CH deformation respectively. The peak at 1225 cm^{-1} referred to the stretching of the ester groups region. The C-O-C peak appeared at 1090 cm^{-1} while the transmittance peaks at

4.2.3 Scanning Electron Microscope (SEM/ SEM-EDX)

Figure 4.6a and 4.6b presents the surface morphologies of some PLLA-HP Mg and PLLA-AZ91 after coating. The average diameter of fibers of PLLA-HP Mg and PLLA-AZ91 were around 429 ± 53 nm. The fibers of HP Mg coated samples (PLLA-HP Mg 1, PLLA-HP Mg 4, PLLA-HP Mg 5 and PLLA-HP Mg 6) and AZ91 coated samples (PLLA-AZ91 2, PLLA-AZ91 4, PLLA-AZ91 5 and PLLA-AZ91 6) have an irregular, undulating morphology with large variations in diameter along a single fiber. This finding was also reported by (Min, You, Kim, Lee, & Park, 2004; Ngiam et al., 2009). According to (Iafisco, Foltran, Sabbatini, Tosi, & Roveri, 2012), this observation was due to non-uniform fibers were more easily to form with high molecular weight PLLA. There were numerous junctions and fibers were found on coated samples. The fiber mats were smooth and beadless showing the bonding of intersecting fibers had created well adherence with metal substrate (Agrawal & Ray, 2001; Deitzel, Kleinmeyer, Harris, & Beck, 2001).

For PLLA-HP Mg 2, PLLA-HP Mg 3 and PLLA-AZ91 3, the fibers had formed bead on the samples. These beads were found to fuse together and solidify into larger molten structure. Although using same electrospinning parameter with other samples, samples had formed beads. There are other parameters affecting electrospinning process such as solution properties, set up variables and ambient condition (Luo, Nangrejo, & Edirisinghe, 2010; Shenoy, Bates, Frisch, & Wnek, 2005; Tan, Inai, Kotaki, & Ramakrishna, 2005). Due to chemical stability of polymer solution used can be degraded over time, the chemical properties of polymer solution also changed (Agarwal, Wendorff, & Greiner, 2008). Polymer degradation will lead to formation of fiber with beads (Liang, Hsiao, & Chu, 2007).

The EDX results shown in Table 4.2 proved that samples were mainly composed of Carbon and Oxygen elements on PLLA-HP Mg and PLLA-AZ91 from Figure 4.6. The atomic concentration of Mg on PLLA-HP Mg was 0.1% while atomic concentration of Mg on PLLA-AZ91 was not detected by EDX. The atomic concentration of Zn was too small and Al also not identified by EDX. This proved that Mg samples were successfully coated with PLLA as C and O are from the polymer coating. Thus the main elements of metal substrate were not traced as it was beneath the surface of PLLA layer.

Table 4.2: EDX analyses of samples surface.

Material	**EDX**
HP Mg	O, Mg
AZ91	O, Mg, Zn, Al
PLLA-HP Mg	C, O
PLLA-AZ91	C, O

4.2.4 Thickness and Adhesion Test

The thickness of PLLA layer on HP Mg samples was determined using microscratch test and the thickness on PLLA-AZ91 was evaluated by surface profiler. Table 4.3 presents the thickness reading and average thickness obtained from both samples, PLLA-HP Mg and PLLA-AZ91. The average thickness of PLLA-HP Mg was 27.07 µm. The average thickness of PLLA-AZ91 was 16.63 µm. It was found that the thickness of PLLA-HP Mg was higher than PLLA-AZ91 even when the electrospinning conditions were consistent. This was due to the surface morphology of AZ91 sample which was smoother compared to HP Mg sample. Surface profiler was a common test use to determine the thickness of coater and substrate. In which a cut was made on the surface of coated sample. The cut need to reach the metal substrate. Then the needle tip of surface profiler machine will run along the top surface and into the cut that was made. The thickness test using surface profiler was similar with previous research by (Dargaville et al., 2013; Xu & Yamamoto, 2012a).

The thickness of PLLA-AZ91 was determined by microscratch test and the schematic illustration to determine the thickness and adhesion strength of PLLA layer on the Mg surface was shown in the Figure 4.7. The thickness using microscratch was based on the penetration depth of the indenter tip until it reached Mg surface (Wang & Guo, 2016). It was reported by (Jiang, Cheng, & Dinesh, 2009), the adhesion strength was based on load applied in which first failure occurred. From microscratch test done to sample PLLA-AZ91, the test was run until distance of 999.78 µm. Then, image of sample was captured and measured using microscope to identify the point where the tip started to scratch the substrate. For this sample, the indenter tip reached the metal substrate at 682.28 µm. At this point, the penetration depth of tip (thickness) was around 16.94 µm ~ 17.75 µm. The load applied was 422.78 mN at this point. The load applied represents the adhesion strength of PLLA on sample. According to previous studies by (Shi, Niu,

Shanshan, Chen, & Li, 2015), the adhesion test was done to determine the strength of coated sample with the metal substrate.

Table 4.3: Thickness reading of PLLA-HP Mg and PLLA-AZ91.

Samples	Thickness (µm)			Average thickness(µm)
PLLA-HP Mg	26.99	27.28	26.94	27.07
PLLA-AZ91	17.75	16.94	15.21	16.63

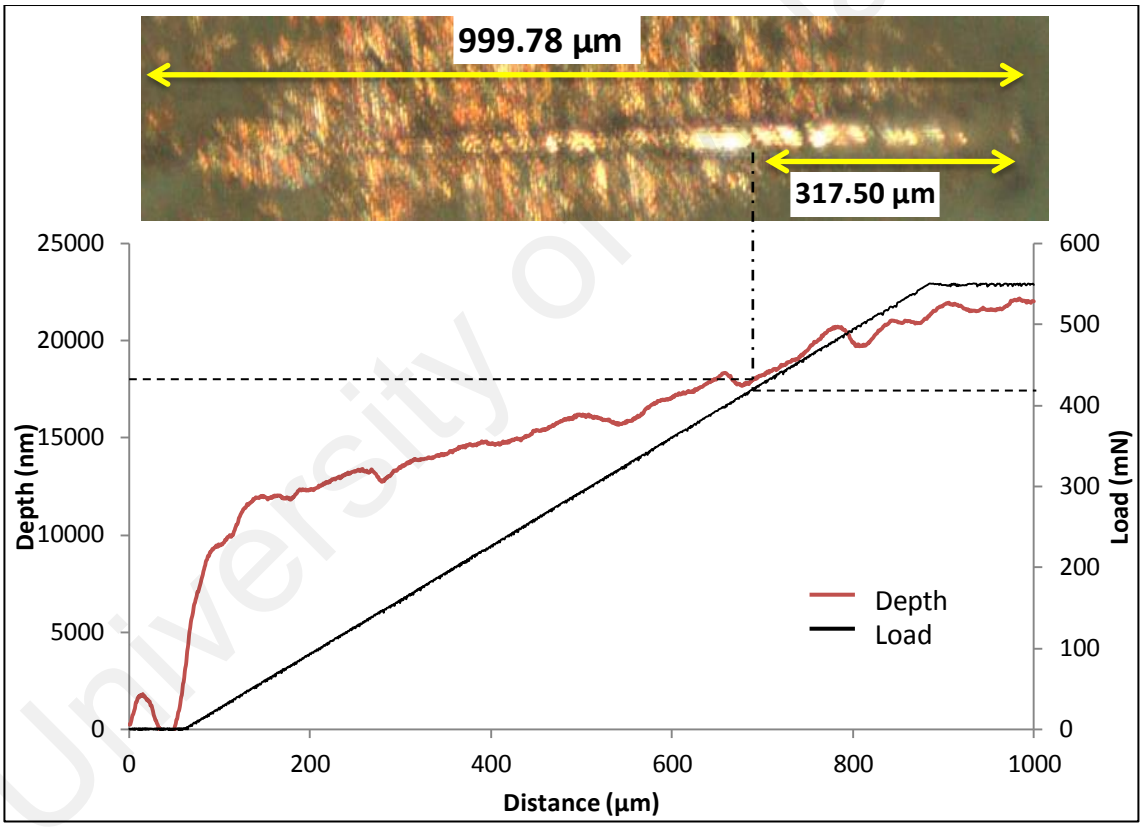

Figure 4.7: Microscracth test on PLLA-AZ91 sample.

To qualify the adhesion result, a standard adhesion test was done by following standard test ASTM 3359. Indeed, this test has been found from research done by (Singer, Distler, & Virtanen, 2014). According to standard method, samples that have thickness below 50 µm, eleventh cut was made on top of coating with each cut was 1 mm apart

from each other. Then, a pressure-sensitive tape was applied on the cuts. After that, the tape was slowly removed from the surface. The remaining percentage of polymer residues on the surface was compared with the standard's categories to qualify the adhesion strength. The adhesion was determined by followed ASTM D3359 method as described above. The adhesion test of the PLLA coating on magnesium surface was in class 0(B). In that category, more than 65% of the coating was removed by the adhesive tape. This indicated weak adhesion strength of the PLLA coating on the Mg surface.

Additional thickness test was done to the sample using FESEM. The thickness of PLLA layer on Mg surface from FESEM was in between 1.81 µm ~ 2.37 µm. The test was done using cold mounting technique which coated sample was leave overnight in Epoxy resin solution. The thickness from FESEM was inaccurate due to PLLA layer dissolve in Epoxy resin (Guo & Li, 2004). Figure 4.8 below shows FESEM cross section of PLLA on the surface of Mg sample. The microscope image from Figure 4.7 and FESEM in the Figure 4.8 was not clear due to charging by oxidized surface by Mg and the resolution applied was impossible to be run higher than 15 kV.

4.3 Corrosion Evaluation

The corrosion evaluation of magnesium immersed in Hank's solution at 37ºC for 14 days was determined by H_2 gas evolution, weight loss rate and morphology evaluation by using SEM-EDX.

4.3.1 Hydrogen Evolution and Weight Loss

Figure 4.9 and 4.10 present the corrosion behaviour of HP Mg, AZ91, PLLA-HP Mg and PLLA-AZ91 with and without hole characterized by hydrogen evolution respectively. In Figure 4.9 and 4.10, open symbol shows hydrogen evolution volume and full symbols shows corresponding pH of the solution. Sextuplicate specimens were used for HP Mg, AZ91, PLLA-HP Mg and PLLA-AZ91. They were designated as 1, 2, 3 for specimens with hole and 4, 5, 6 for specimens without hole. HP Mg 2 and PLLA-AZ91 1 have been omitted due to technical error. During immersion test done to both samples, the specimens were detached from fishing line. Thus, to report hydrogen evolution volume and the corrosion rate, P_{AH} for these samples was impossible and inaccurate.

The hydrogen evolution volume of all samples increased with the immersion time. The same result was also reported by previous studies (Y. Chen et al., 2013; Hänzi, Gerber, Schinhammer, Löffler, & Uggowitzer, 2010). Figure 4.9a shows the hydrogen evolution volume of HP Mg samples with hole while Figure 4.9b presents the hydrogen evolution volume of PLLA-HP Mg with hole for 14 days of immersion time. From Figure 4.9a and 4.9b, both coated and uncoated samples HP Mg with hole does not have incubation period. The hydrogen evolution rate of coated sample was slightly higher than uncoated HP Mg sample.

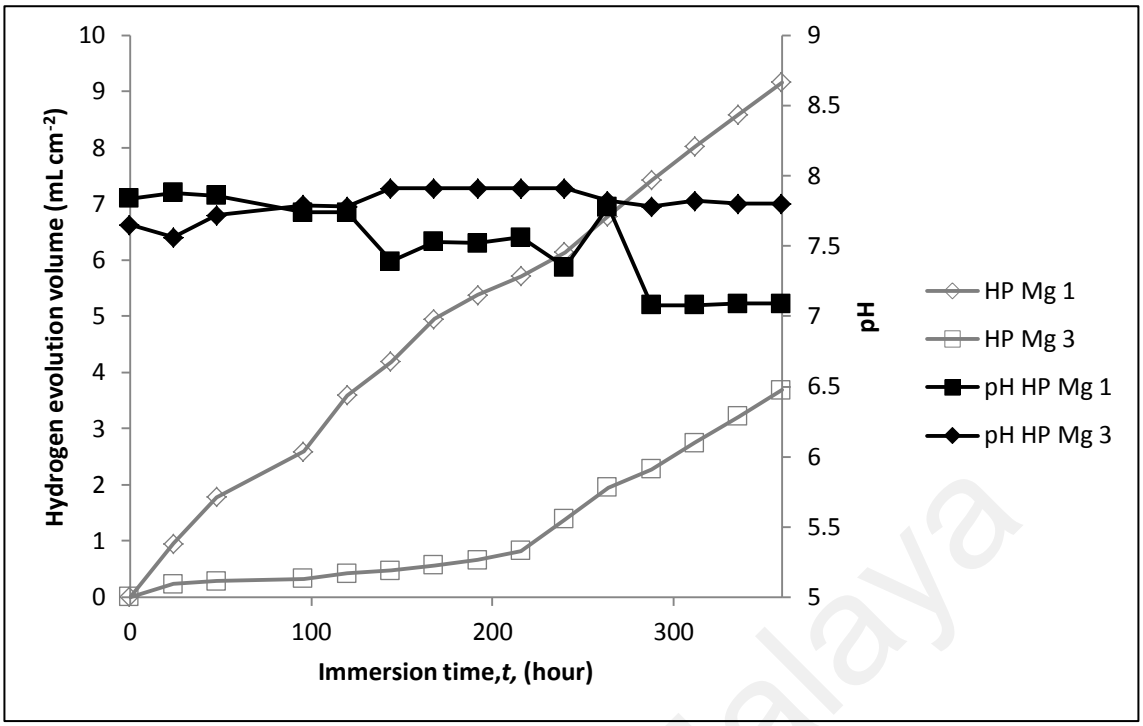

Figure 4.9a: Hydrogen evolution of HP Mg (with hole) in Hank's solution.

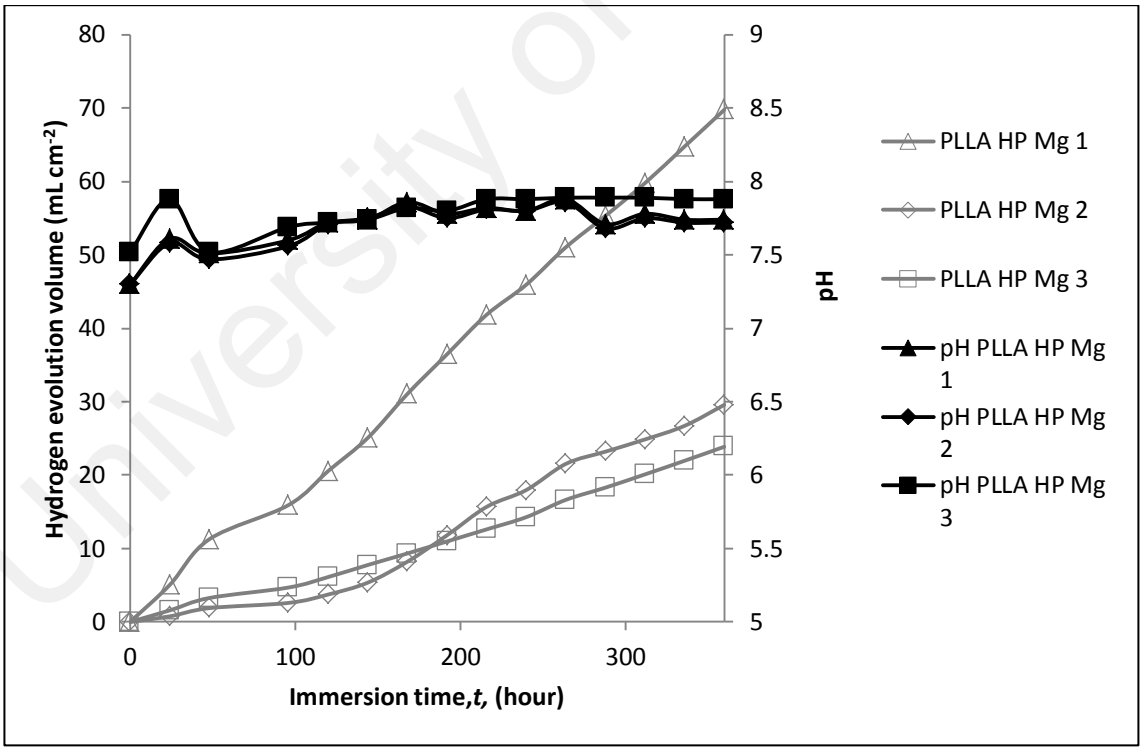

Figure 4.9b: Hydrogen evolution of PLLA-HP Mg (with hole) in Hank's solution.

Figure 4.9 shows the hydrogen evolution data of samples HP Mg and AZ91 (coated and uncoated) with hole against immersion time. The hydrogen evolution volume of all HP Mg samples with hole gradually increased except HP Mg 3. The hydrogen evolution of HP Mg increased slowly then rapidly increased after 225 hr. The total hydrogen evolved of HP Mg 1 and HP Mg 3 were under 10 ml/cm^2. The volume of hydrogen evolves of PLLA-HP Mg 2 and PLLA-HP Mg 3 on Figure 4.9b show similar patterns. The hydrogen evolutions of all PLLA-HP Mg with hole were slightly higher than uncoated HP Mg with hole. It has been stated by previous finding that as Mg surface is unstable where surface modification should improve its stability (Nudelman, Lausch, Sommerdijk, & Sone, 2013; Zhou & Lee, 2011). However, modification used can be toxic and may not sufficiently improve the degradation behaviour of Mg (Mendonça, Mendonça, Aragao, & Cooper, 2008). This also may attribute to the polymer on the surface gradually become more hydrophilic in aqueous environments (Abdal-hay, Tijing, & Lim, 2013; Krikorian & Pochan, 2003; R. Zhang & Ma, 1999). Moreover, as the coating of PLLA on the samples were not well coated on the hole area, thus the stagnant of oxygen beneath the coating accelerate the corrosion to happened.

Figure 4.9c and 4.9d shows the hydrogen evolution of AZ91 and PLLA-AZ91 with hole respectively. The hydrogen evolution rate of PLLA-AZ91 samples was lower than uncoated AZ91. The graphs show all samples of AZ91 with hole both coated and uncoated did not have incubation period except AZ91 3 and PLLA-AZ91 2. The incubation period of AZ91 3 was up until 125 hr while the incubation period of PLLA-AZ91 2 was up until 100 hr.

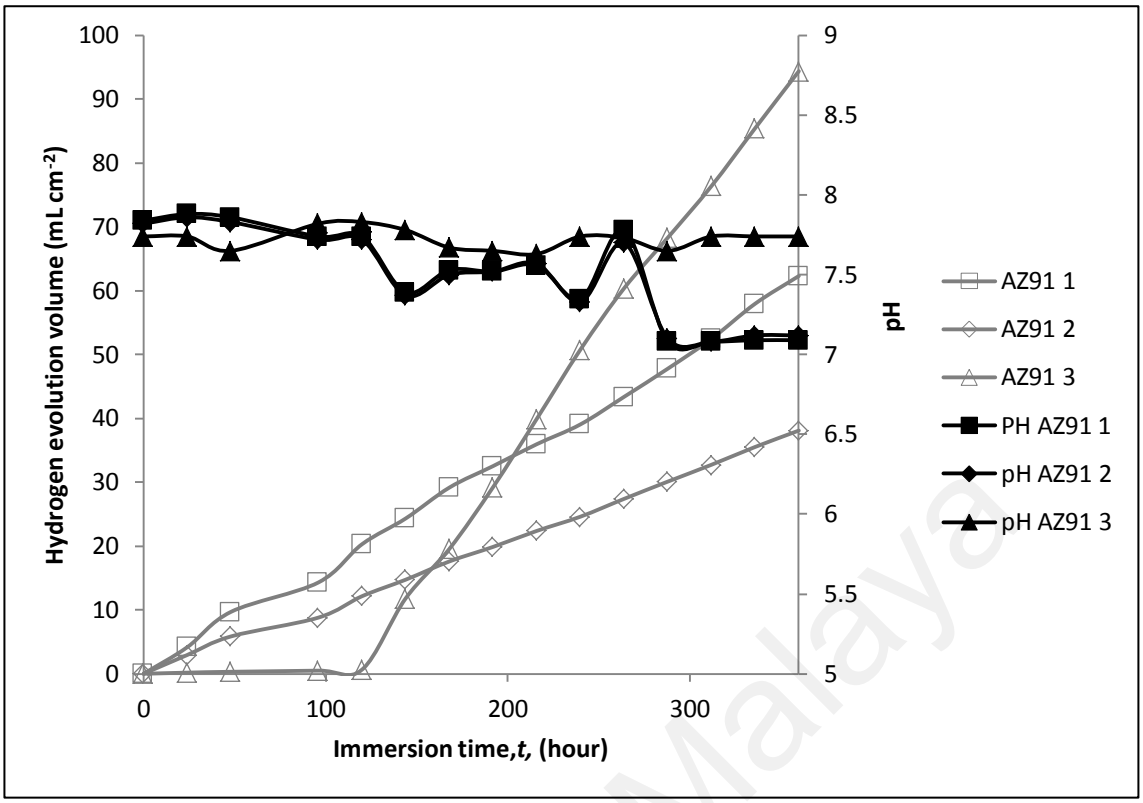

Figure 4.9c: Hydrogen evolution of AZ91 (with hole) in Hank's solution.

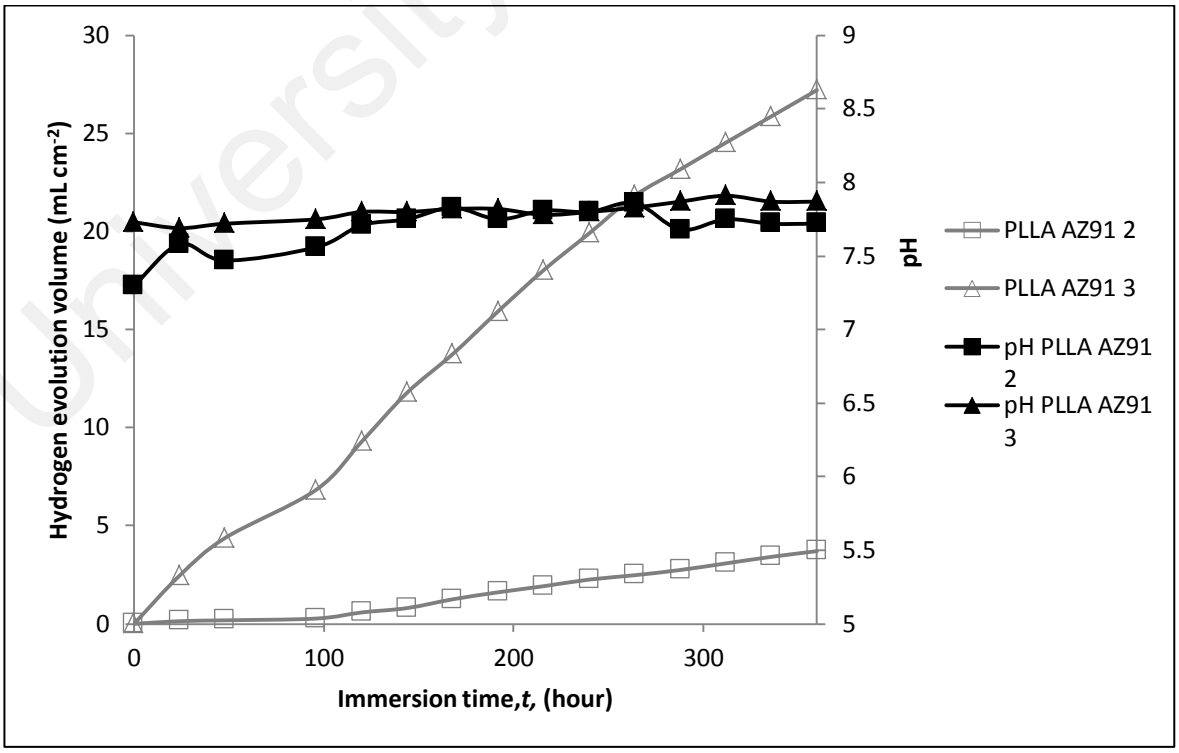

Figure 4.9d: Hydrogen evolution of PLLA-AZ91 (with hole) in Hank's solution.

The hydrogen volumes of uncoated AZ91 with hole were higher than PLLA-AZ91 samples. All samples with hole of PLLA-AZ91 show different trend from PLLA-HP Mg with hole. All samples did not have incubation period except AZ91 3 and PLLA-AZ91 2. The rate was remained low and then increased with increasing immersion duration and typically reached a steady state value during the incubation period. The corrosion rate of AZ91 3 had quickly increases after incubation period whereas PLLA-AZ91 2 increased moderately. AZ91 3 had the highest total hydrogen evolution volume in comparison with other uncoated AZ91 samples even though it was initially incubated. The research by (Lamaka et al., 2017) reported that when lactic acid tested on the surface of AZ91, its shows that the monomer of lactic acts as inhibitors. Thus, it retards the crevice corrosion of PLLA-AZ91 with hole.

Figure 4.10a and 4.10b present hydrogen evolution of HP Mg and PLLA-HP Mg without hole respectively. From the figures, two out of triplicate samples shows similar trend. All HP Mg samples (coated and uncoated) without hole have incubation period except HP Mg 4. The hydrogen evolution volume of coated samples remained low throughout the immersion duration.

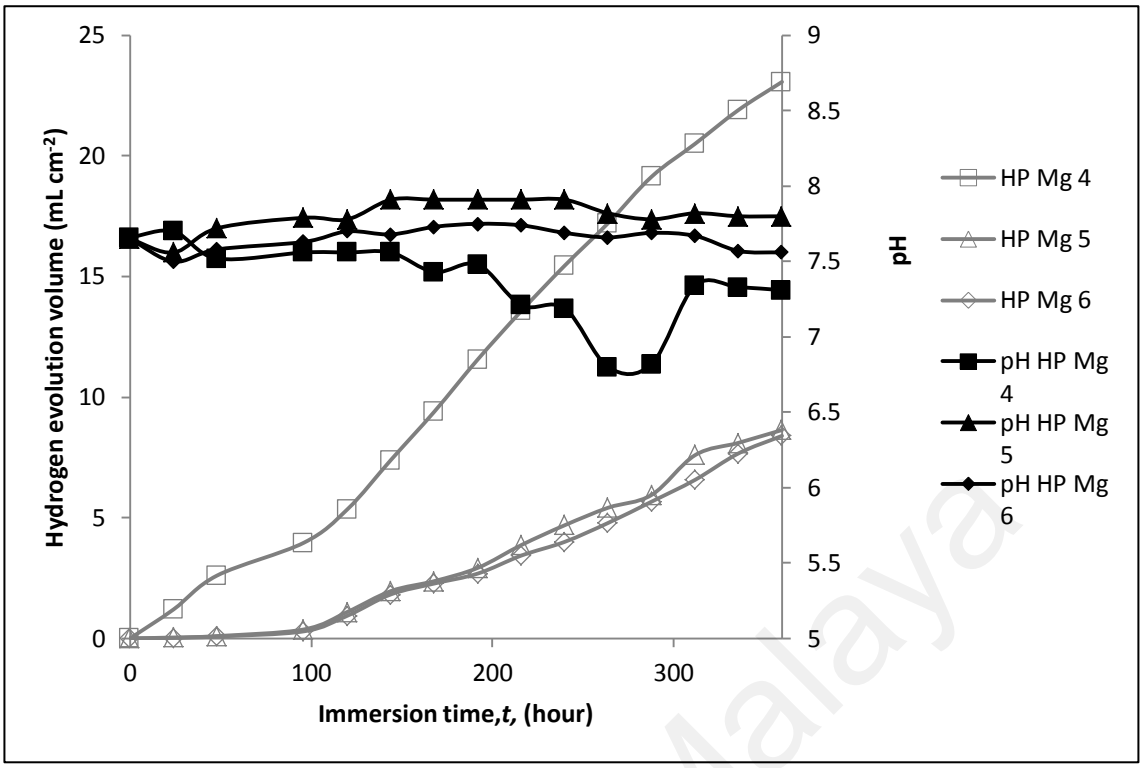

Figure 4.10a: Hydrogen evolution of HP Mg (without hole) in Hank's solution.

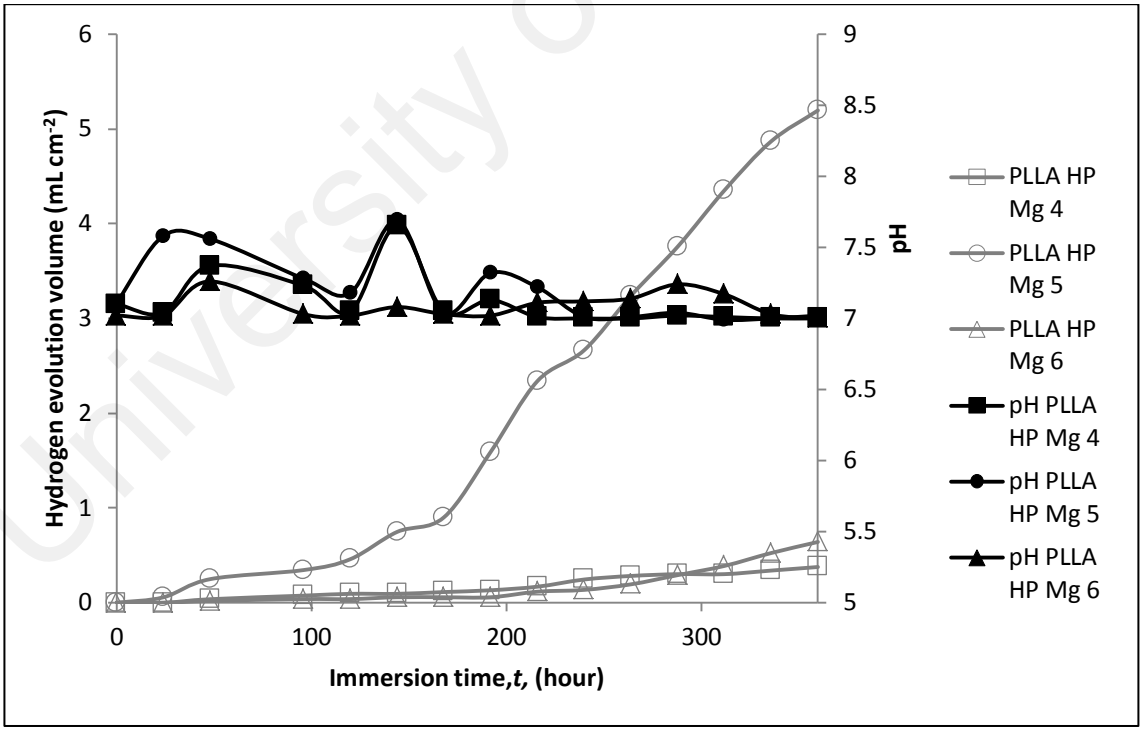

Figure 4.10b: Hydrogen evolution of PLLA-HP Mg (without hole) in Hank's solution.

All samples of HP Mg and AZ91 (coated and uncoated) without hole had incubation period except HP Mg 4. The volume of hydrogen evolves of HP Mg 4 rapidly increased with immersion time until 23 ml/cm^2. The results showed similar trend with previous study (Atrens, Liu, & Zainal Abidin, 2011). Two samples PLLA-HP Mg 4 and PLLA-HP Mg 6 had the longest incubation period up to 200 hr. The incubation period was shortest for PLLA-HP Mg 5. PLLA-HP Mg 5 fluctuates increased after incubated up to 25 hr. The incubation periods of both uncoated HP Mg were up to 100 hr except for HP Mg 4. In comparison with two other uncoated HP Mg, HP Mg 4 had the highest total hydrogen evolution volume.

Figure 4.10c and 4.10d show that both coated and uncoated samples AZ91 without hole have incubation period. The hydrogen evolution volume of coated samples tends to remained low while uncoated samples gradually increase with immersion time.

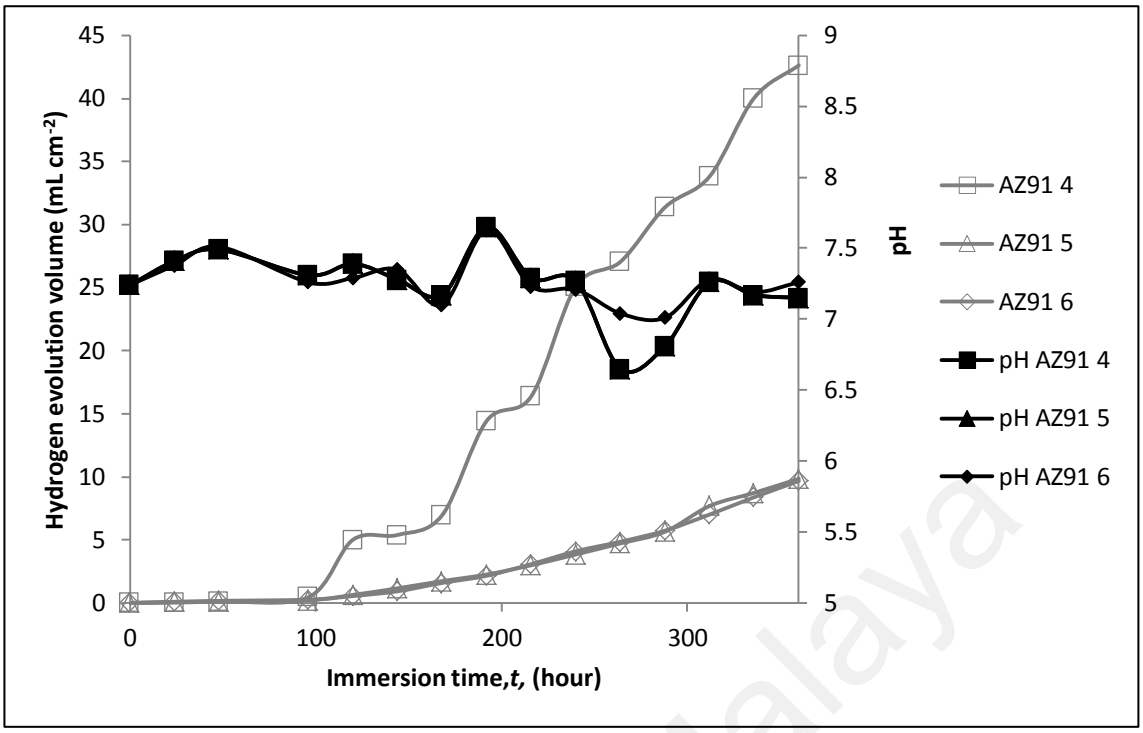

Figure 4.10c: Hydrogen evolution of AZ91 (without hole) in Hank's solution.

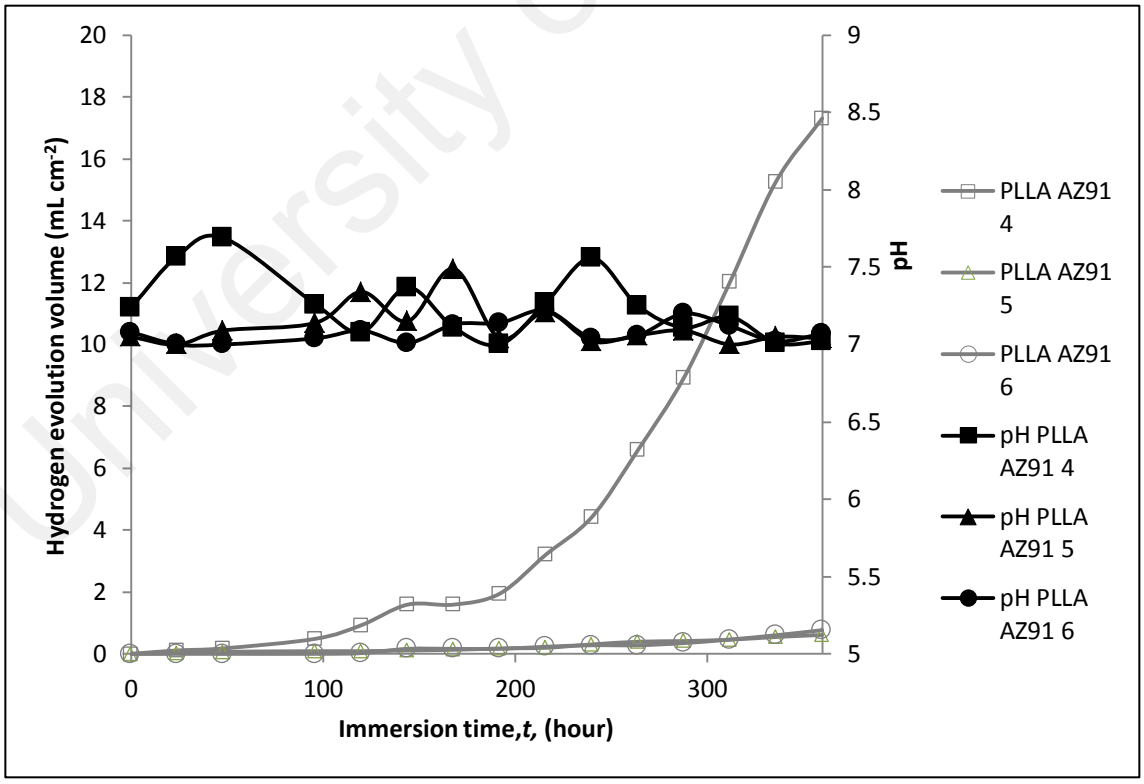

Figure 4.10d: Hydrogen evolution of PLLA-AZ91 (without hole) in Hank's solution.

AZ91 4 had the higher corrosion rate in comparison with other uncoated AZ91 even though it had similar incubation period. The incubation period of all uncoated AZ91 samples was up to 100 hr. The hydrogen evolution volume of PLLA-AZ91 5 and PLLA-AZ91 6 increased slowly throughout 14 days of immersion test after having incubation period up to 125 hr. The hydrogen evolution volume of PLLA-AZ91 4 slightly increased after incubated until 50 hr before increased rapidly. Two out of triplicate samples from each Mg samples without hole showed similar behaviour. The hydrogen evolutions of coated samples (PLLA-HP Mg and PLLA-AZ91) without hole are lower than the hydrogen volume of uncoated samples without hole.

Table 4.4 shows the weight loss data, $W_{L,}$ the corresponding corrosion rate, P_W, the hydrogen evolution rate, V_{TH}, and the corresponding corrosion rate, P_{AH} for specimens HP Mg, AZ91, PLLA-HP Mg and PLLA-AZ91 in Hank's solution for 14 days. From table, it can be seen that the difference of average corrosion rate, P_{AH} of AZ91 and PLLA-AZ9 without hole was 2.36 mm y^{-1}. The difference of P_{AH} of HP Mg and PLLA-HP Mg without hole was 1.84 mm y^{-1}. For sample with hole, AZ91 and PLLA-AZ91 had a difference of 8.16 mm y^{-1}. The difference of average corrosion rate, P_{AH} of PLLA-HP Mg was negative as sample of PLLA-HP Mg with hole have higher hydrogen evolution than HP Mg. The effectiveness percentage of coating applied to PLLA-HP Mg (without hole), PLLA-AZ91 (without hole) and PLLA-AZ91 (with hole) was 84%, 70% and 76% respectively.

. **Table 4.4:** Corrosion rate of HP Mg, AZ91, PLLA-HP Mg and PLLA-AZ91 in Hank's solution.

Material		Immersion period (hour)	W_L (mg cm^{-2} d^{-1})	P_W (mm y^{-1})	V_{TH} (mL cm^{-2} d^{-1})	P_{AH} (mm y^{-1})
HP Mg	1	336	0.38	0.80	0.65	1.49
	3	336	0.35	0.74	0.26	0.60
	4	336	0.88	1.84	1.65	3.76
	5	336	0.38	0.79	0.62	1.41
	6	336	0.37	0.78	0.60	1.37
PLLA-HP Mg	1	336	0.93	1.96	4.98	11.36
	2	336	0.92	1.92	2.11	4.82
	3	336	0.89	1.88	1.70	3.89
	4	336	0.26	0.55	0.03	0.06
	5	336	0.36	0.75	0.37	0.85
	6	336	0.32	0.68	0.05	0.10
AZ91	1	336	0.93	1.95	4.45	10.14
	2	336	0.92	1.93	2.72	6.20
	3	336	0.97	2.03	6.74	15.36
	4	336	0.92	1.93	3.04	6.94
	5	336	0.51	1.07	0.70	1.60
	6	336	0.49	1.03	0.69	1.57
PLLA-AZ91	2	336	0.35	0.74	0.26	0.60
	3	336	0.90	1.89	1.94	4.43
	4	336	0.56	1.18	1.24	2.82
	5	336	0.29	0.62	0.04	0.10
	6	336	0.32	0.68	0.05	0.12

From Table 4.4, the average corrosion rates, P_W and corrosion rate from hydrogen evolved, P_{AH} have good agreement eventhough the corrosion rate obtained from the weight loss were smaller than the corrosion rates obtained from hydrogen evolution volume for all samples. This is because after immersion test, all samples were cleaned with chromic acid. However, it was observed PLLA coating still attached to the surface of Mg substrate. This finding was similar with the research work by (Hort et al., 2010). Table 4.3 signify that overall corrosion rate of Mg samples with hole ranked as: HP Mg < PLLA-AZ91 < PLLA-HP Mg < AZ91. The corrosion rate of Mg samples without hole ranked as: PLLA-HP Mg < PLLA-AZ91 < HP Mg < AZ91. This may be attributed to the greater impact of PLLA coating layer that successfully protecting the surface (Zainal Abidin, Martin, & Atrens, 2011).

Samples without hole and well coated with PLLA have lower volume of hydrogen evolution. It proved that surface modification onto Mg surface with PLLA possibly reduced the volumes of hydrogen evolved and also reduced the corrosion rates of Mg. This result is also suggested by previous studies in which by coating the anodic (metal) can reduce the corrosion rate (Song, 2007). AZ91 3 (with hole) and AZ91 4 (without hole) have the shortest incubation period and rapidly rose after 120 hr, this behaviour similar with previous observation of corrosion behaviour for Mg alloys. It is predicted that the initiation and propagation of the heterogeneous corrosion is a stochastic process and the variability possibly because AZ91 was die casting and some rare impurities particles, thus the resultant corrosion rate is much greater than normal samples (Ambat, Aung, & Zhou, 2000; Pardo et al., 2008). In general, corrosion rate of Mg alloy tend to be greater than high purity Mg due to alloying metal (impurities) but with surface coating, corrosion resistance of alloy can be improved particularly during initial stages as it successfully delayed biodegradation of substrate (Rojaee, Fathi, & Raeissi, 2013a).

4.3.2 Solution pH

Figure 4.9 and 4.10 also plot the solution pH during the immersion test. The full symbols on the graph represented the pH value. The pH was in the range 7.0-7.8 for both coated and uncoated high purity magnesium and its alloys. The pH was successfully maintained by bubbling CO_2 with partial pressure of 0.009 atm into Hanks' solution.

As shown in both figures, the pH of uncoated HP Mg and AZ91 started at around 7.8 and decreased with increased immersion time while both coated HP Mg and AZ91 remained in between 7.0 to 7.88. This means corrosion reaction for uncoated Mg and alloy tend to be active in the beginning of immersion time compared to the coated specimen as it is protected by layer of polymer coating (Hiromoto, Yamamoto, Maruyama, Somekawa, & Mukai, 2008). Hence, the corrosion reaction tends to slow down at the beginning of immersion time. Certain conditions of the environment play an important role for the corrosion behaviour of metals in surface reaction. Metal corrosion and biological reaction can influence the pH changes. Surface alkalization due to Mg dissolution can lead to high alkalinity (Razavi et al., 2014). It means pH will increase upon Mg corrosion in which hydrogen gas and oxygen gas reduction play role.

4.3.3 Surface Morphology by SEM-EDX

Figure 4.11 shows the surface condition of HP Mg, AZ91, PLLA-HP Mg and PLLA-AZ91 after immersion test was for 14 days and before corrosion product removal. Figure 4.12 shows the surface morphologies of HP Mg, AZ91, PLLA-HP Mg and PLLA-AZ91 after immersion tests were done and before removal of corrosion product using SEM-EDX respectively. Table 4.5 shows overall EDX analyses of corrosion product on the surface after immersion test.

For uncoated samples shown in the Figure 4.11, there were white corrosion products on the substrate surface. It was expected as hydroxapatite, heavily carbonated apatite and slightly carbonated apatite form. It was confirmed through EDX done to the samples as shown in Table 4.5. It can be verified from the research work by (Hiromoto, 2015).

For coated samples, the PLLA layer still attached to the samples surface. It can be clearly seen that corrosion started at the edge of sample where delamination occurred and caused the breakdown of coated layer. The findings were similar with previous research by (Gu, Bandopadhyay, Chen, Ning, & Guo, 2013). As coating should delay the degradation of Mg, corrosion will under attack once the coating no longer acts as protective layer to Mg.

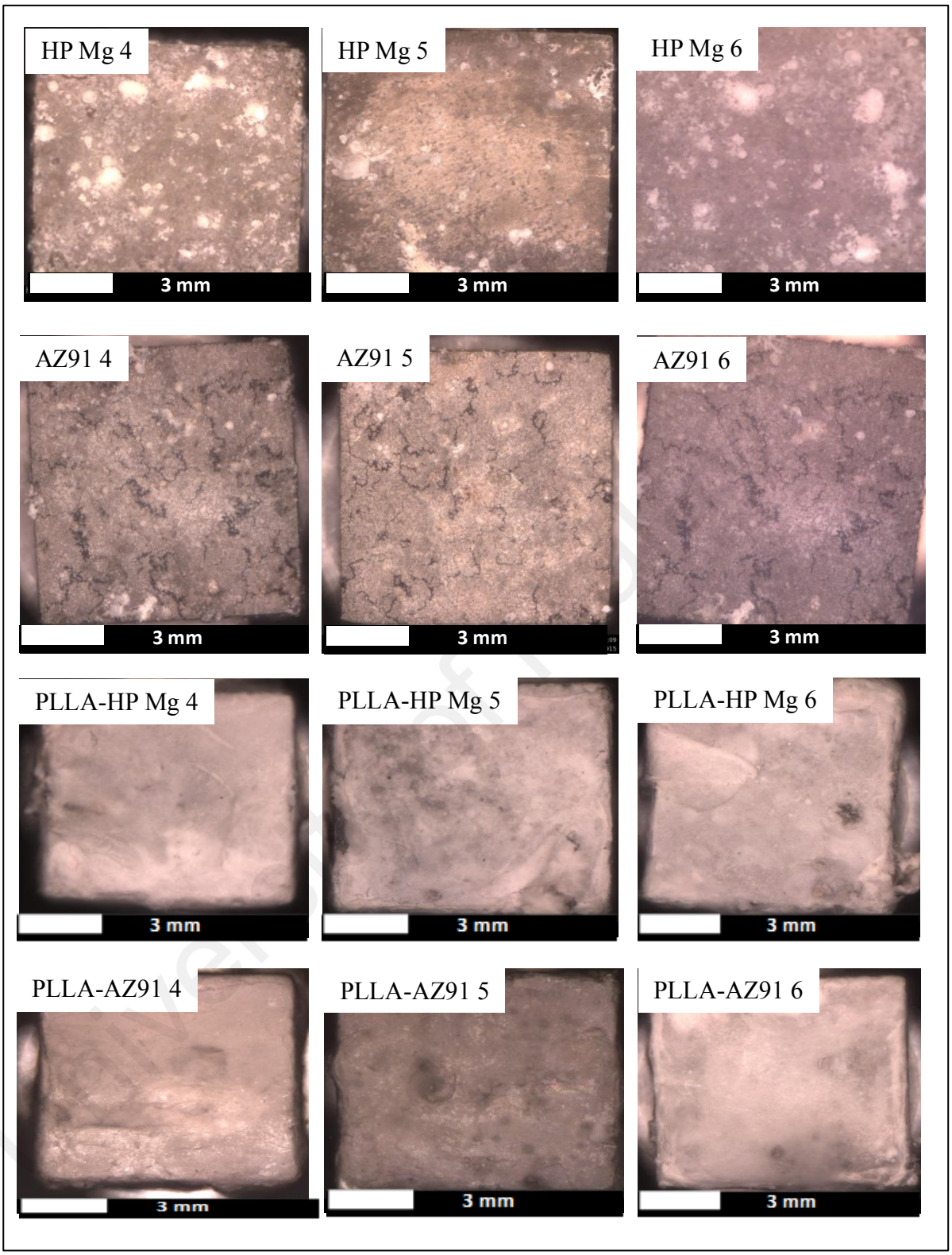

Figure 4.11: Surface appearance of samples HP Mg, AZ91, PLLA-HP Mg and PLLA-AZ91 after immersion test for 14 days and before corrosion product removal.

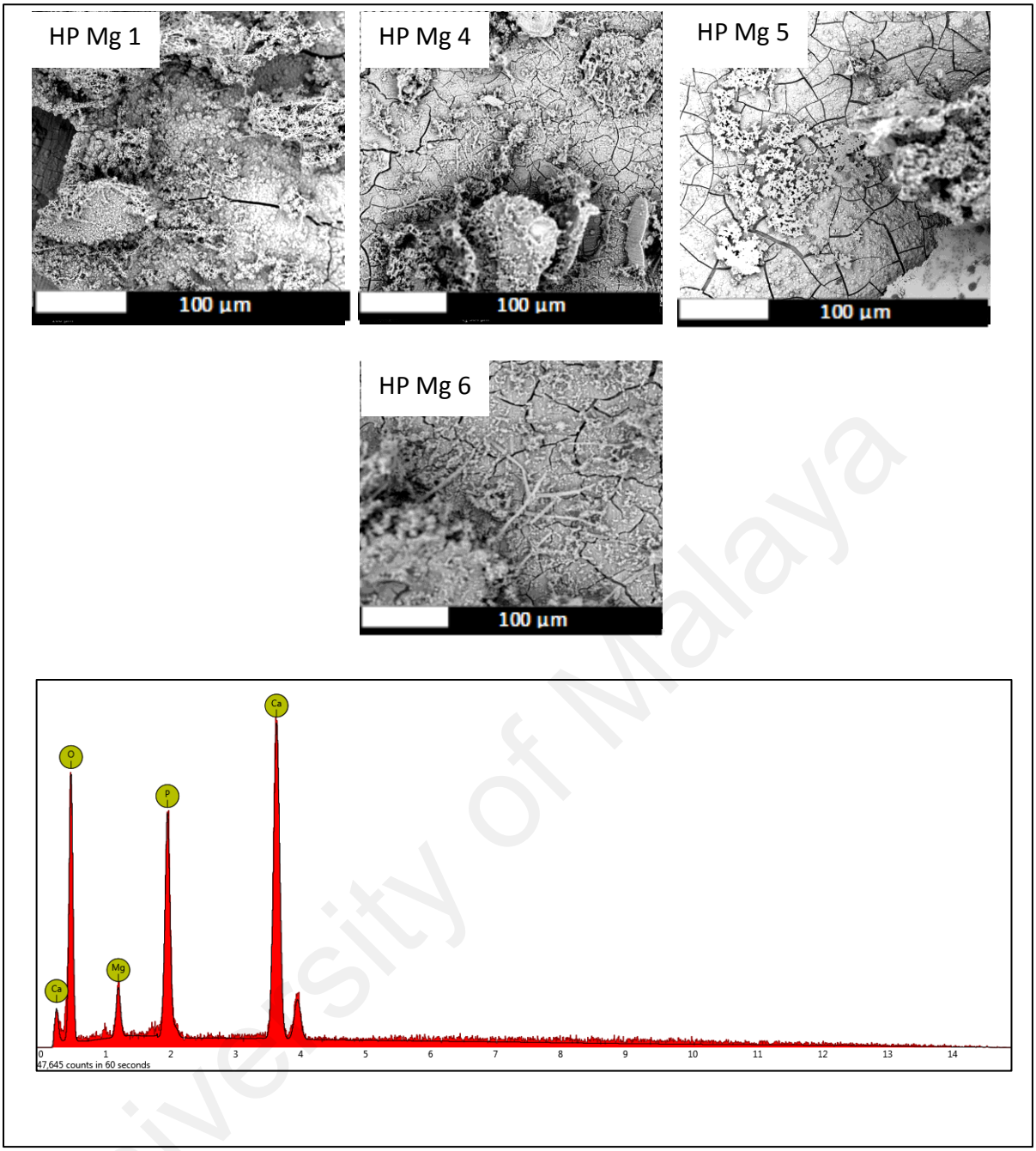

Figure 4.12a: SEM surface morphologies of HP Mg after immersion test without corrosion removal.

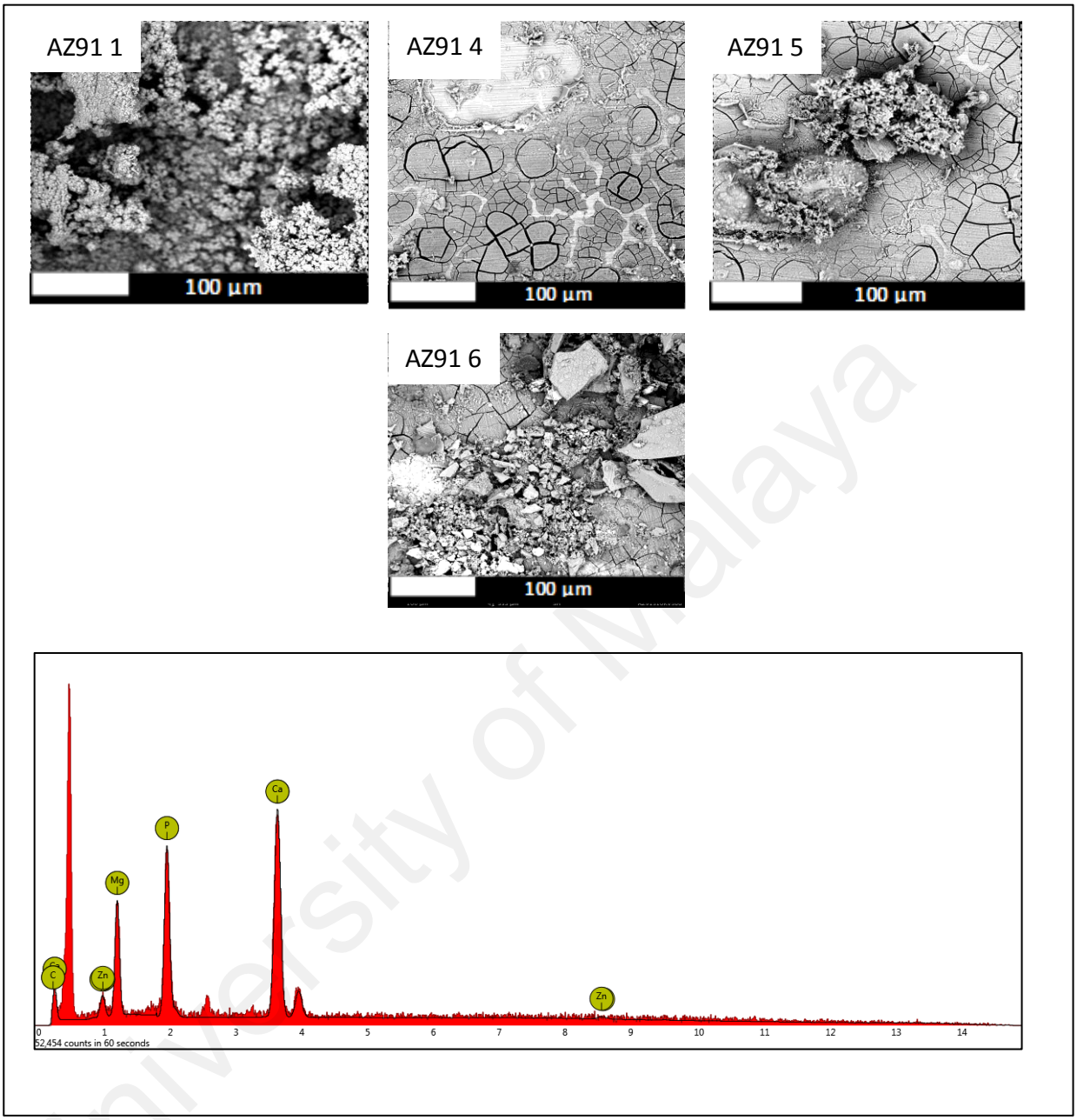

Figure 4.12b: SEM surface morphologies of AZ91 after immersion test without corrosion removal.

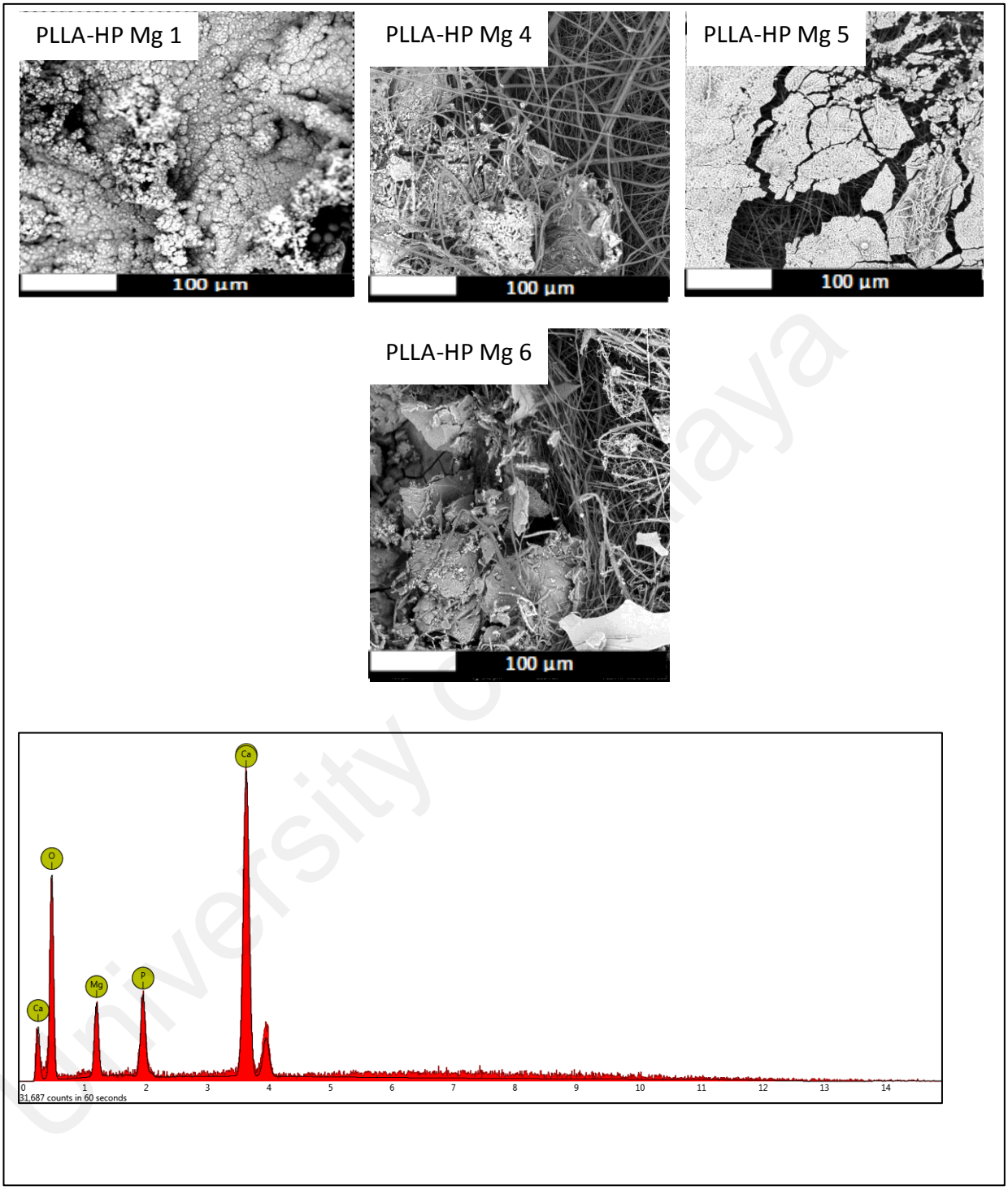

Figure 4.12c: SEM surface morphologies of PLLA-HP Mg after immersion test without corrosion removal.

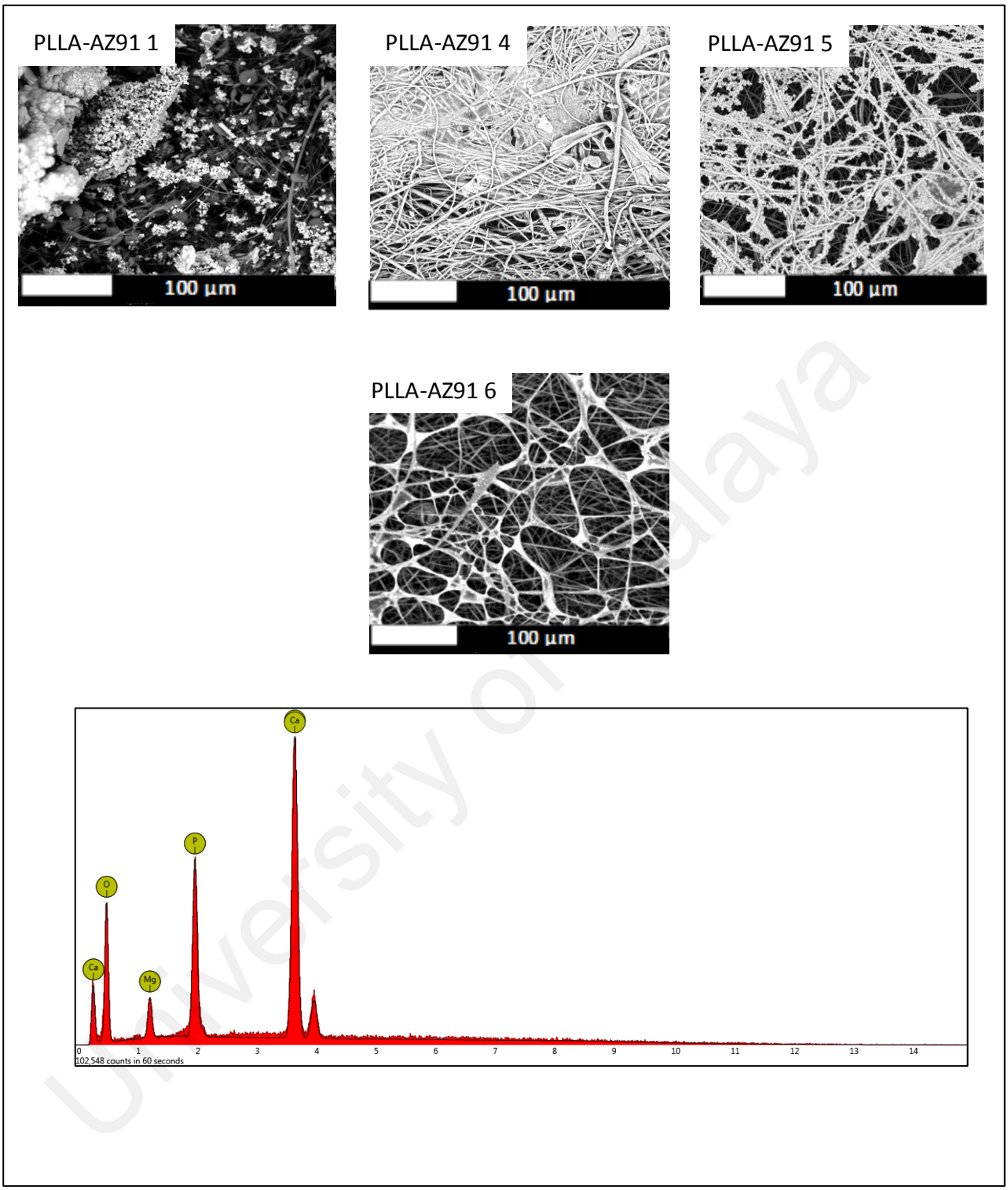

Figure 4.12d: SEM surface morphologies of PLLA-AZ91 after immersion test without corrosion removal.

Table 4.5: EDX analyses of corrosion products on the surface.

Material	EDX
HP Mg	Ca, O, Mg, P
AZ91	Ca, Mg, Cl, P, C, Zn
PLLA-HP Mg	Ca, P, O, Mg
PLLA-AZ91	Ca, O, P, Mg , Zn, Al

From SEM photo of surface morphologies (Figure 4.12), some cracks appear in the corrosion products and this is due to the shrinkage of the corrosion product during drying process. This was already mentioned by (Pardo, Merino, Coy, Arrabal, et al., 2008).

The EDX spectra proved that Ca/P might cause formation of hydroxyapatite and it can be speculated that Mg hydroxide, amorphous Ca/P and Mg apatite amorphous compound deposited on surface where these compound comes from Hank's solution. The chemical reaction in Hank's solution were reported by (Sui & Cai, 2006) and (Xu et al., 2009). Interaction of Mg with Calcium, carbonate and Phosphate ions which are chemical compound from Hanks' solution shown in Eq. (4.1) and Eq. (4.2):

$$Mg^{2+} + Ca^{2+} + (PO_4)^{3-} = Ca_3Mg_3(PO_4)_4 \quad (4.1)$$

$$Mg^{2+} + (CO_3)^{2-} = MgCO_3 \quad (4.2)$$

In Hank's solution, corrosion occured due to oxide film breakdown and the attack onto the weak part of oxide film and reached the surface of Mg. When polymer coated onto Mg, we expected that, it would provide longer incubation period during the initial stage of immersion (Yamamoto & Hiromoto, 2009).

4.3.4 Corrosion Product Evaluation

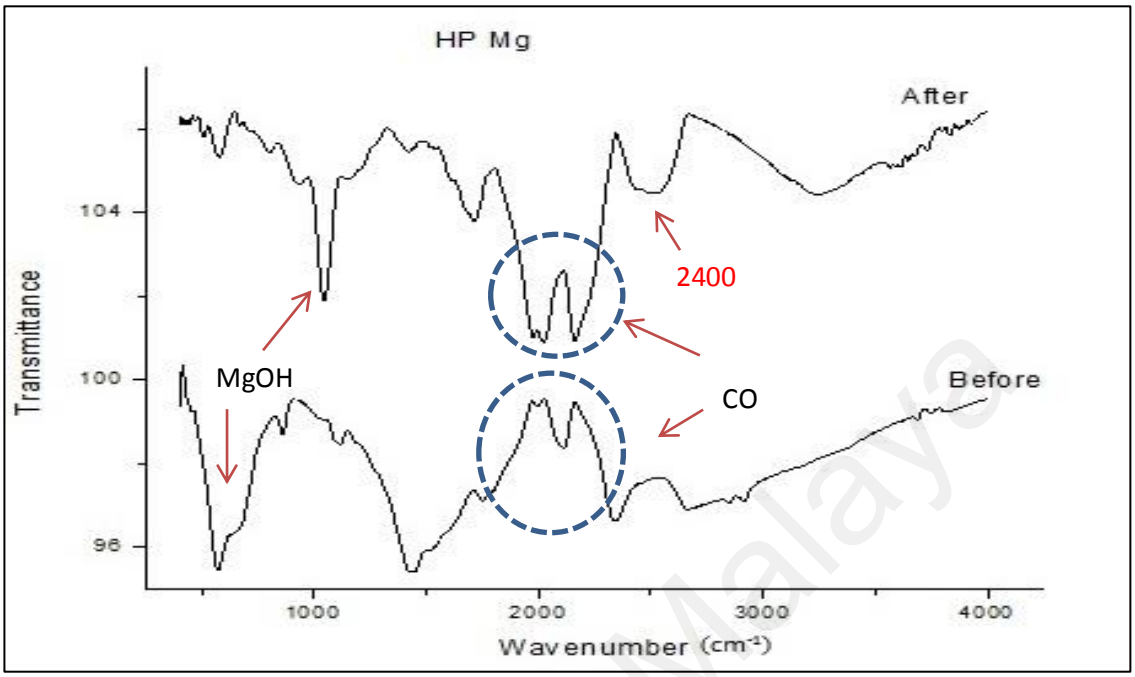

Figure 4.13a: FTIR on corrosion product on HP Mg compared to HP Mg before immersion test.

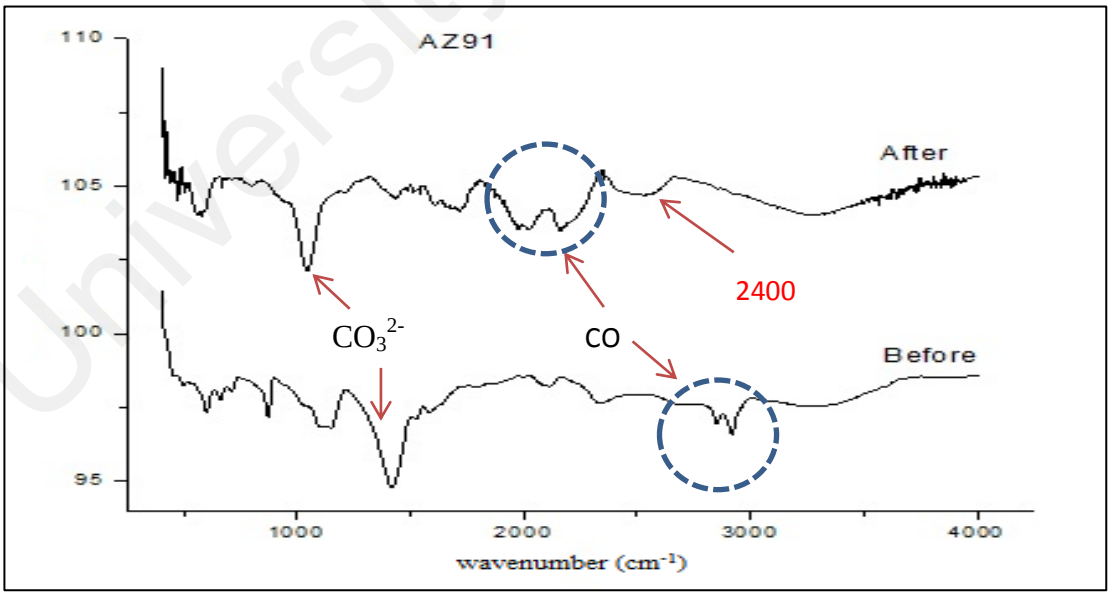

Figure 4.13b: FTIR on corrosion product on AZ91 compared to AZ91 before immersion test.

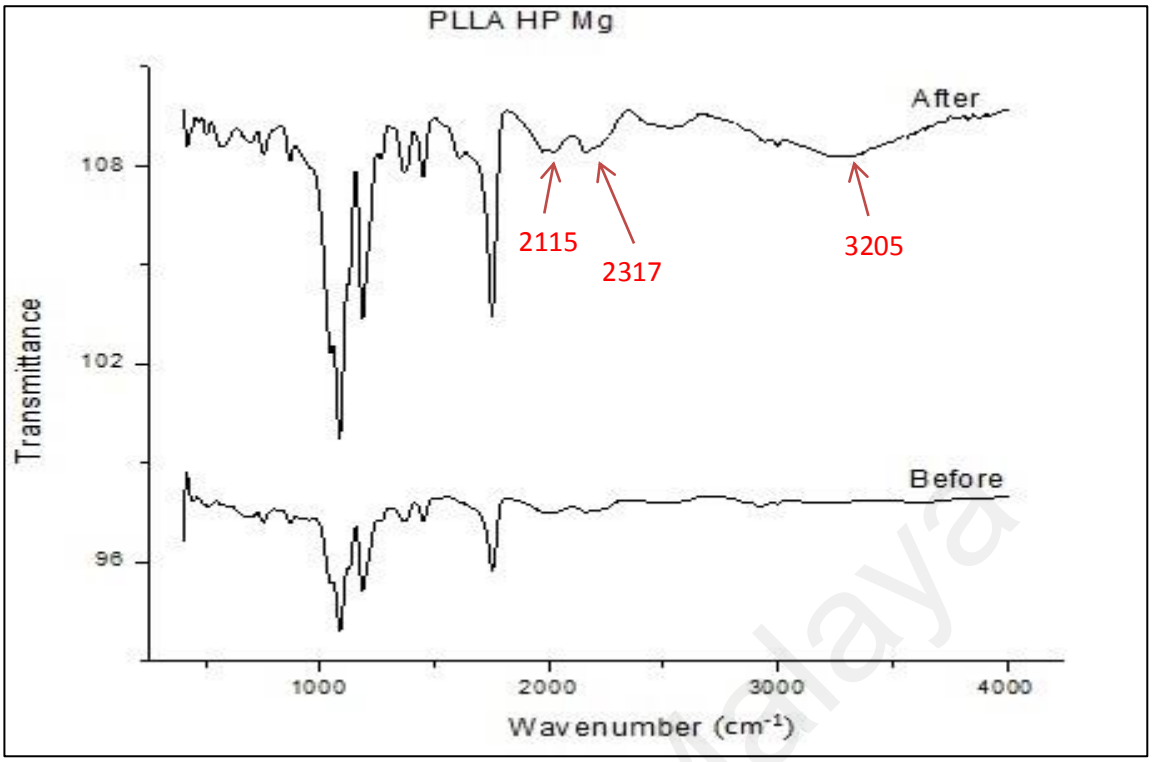

Figure 4.13c: FTIR on corrosion product on PLLA-HP Mg compared to PLLA-HP Mg before immersion test.

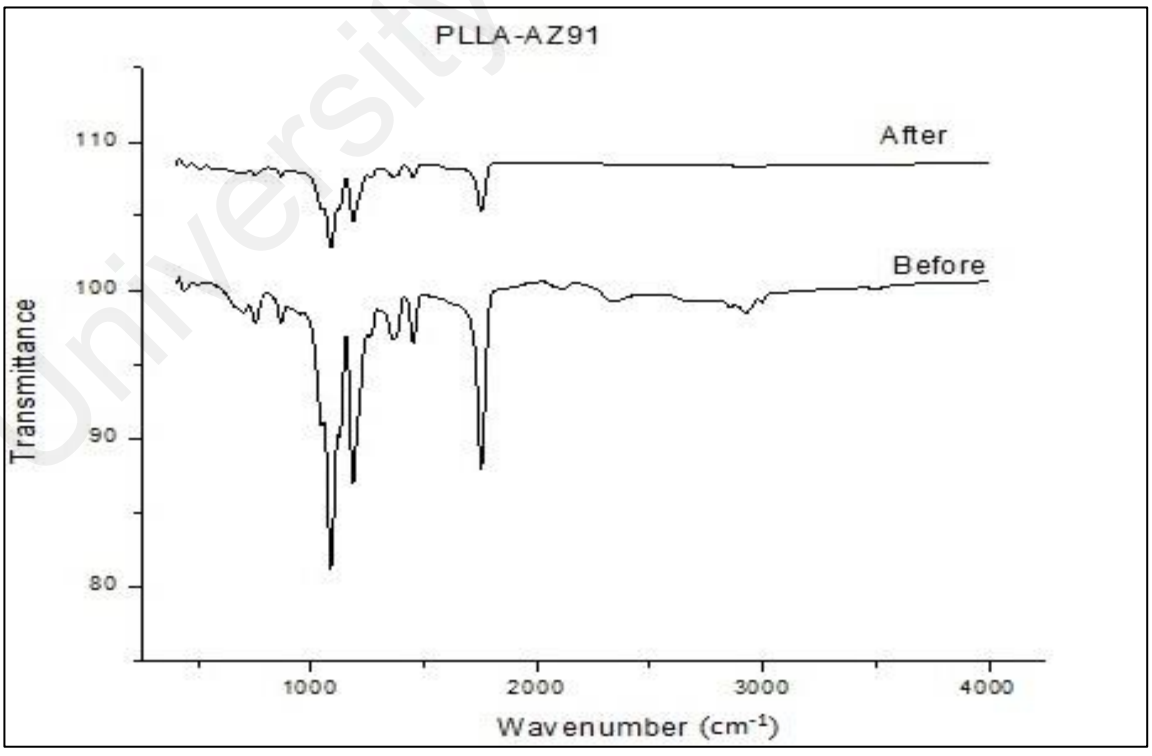

Figure 4.13d: FTIR on corrosion product on PLLA-AZ91 compared to PLLA-AZ91 before immersion test.

Figure 4.13 present FTIR spectrum on the corrosion product of HP Mg, AZ91, PLLA-HP Mg and PLLA-AZ91. Corrosion product was obtained by scraping Mg surface before cleaning with chromic acid (Cai et al., 2011). The FTIR results of corrosion product were compared with FTIR before immersion test. From Figure 4.13a and Figure 4.13b, there were few new peaks and some peaks were shifted from their original position. The transmittance bands at 3316 cm^{-1} and 3348 cm^{-1} are attributed to the OH^- peaks. The peaks at shoulder below 1000 cm^{-1} were determined as Mg(OH) and the peak was shifted from HP Mg before immersion test. Double peaks CO carboxylic acid were appeared at 2179 cm^{-1} and 2000 cm^{-1} in corrosion product of HP Mg while for corrosion product of AZ91, double peaks appeared at 2202 cm^{-1} and 2000 cm^{-1}.. The sharp peak at 1052 cm^{-1} on HP Mg corrosion product and 1059 cm^{-1} on AZ91 corrosion product were identified as CO_3^{2-}. The double peaks CO carboxylic acid and CO_3^{2-} peaks also shifted from peaks before immersion test. These were attributed to hydromagnesite band. These peaks were shifted from the original peaks at 1426 cm^{-1}. Transmittance band at 598 cm^{-1} and at 595 cm^{-1} were assigned to P-Cl region. It is also reported by (Berzina-Cimdina & Borodajenko, 2012) that peak below 600 cm^{-1} belongs to phosphate group. From both figures, new peak was found at transmittance band 2400 cm^{-1}which belongs to adsorbed water. Figure 4.13c and 4.13d show the FTIR spectrum of corrosion product on PLLA HP Mg and PLLA-AZ91. There were new peaks appeared at 2215 cm^{-1}, 2317 cm^{-1} and 3205 cm^{-1}. The new double peaks at 2215 $cm^{-1}$and 2317 cm^{-1} were attributed to adsorbed water while broad peak at 3205 cm^{-1} identified as OH^- stretch peaks. When compared FTIR spectra of corrosion product of PLLA-HP Mg and PLLA-AZ91 after coating before immersion test, there were no significant difference in terms of appeared peaks. The peaks belonged to PLLA layer that formed on the sample surface (J.-P. Chen & Su, 2011). The differences were the intensity of the peaks. The determination of corrosion product of coated HP Mg and

AZ91 were hindered by the PLLA layer itself. This was due to low corrosion happened beneath the layer.

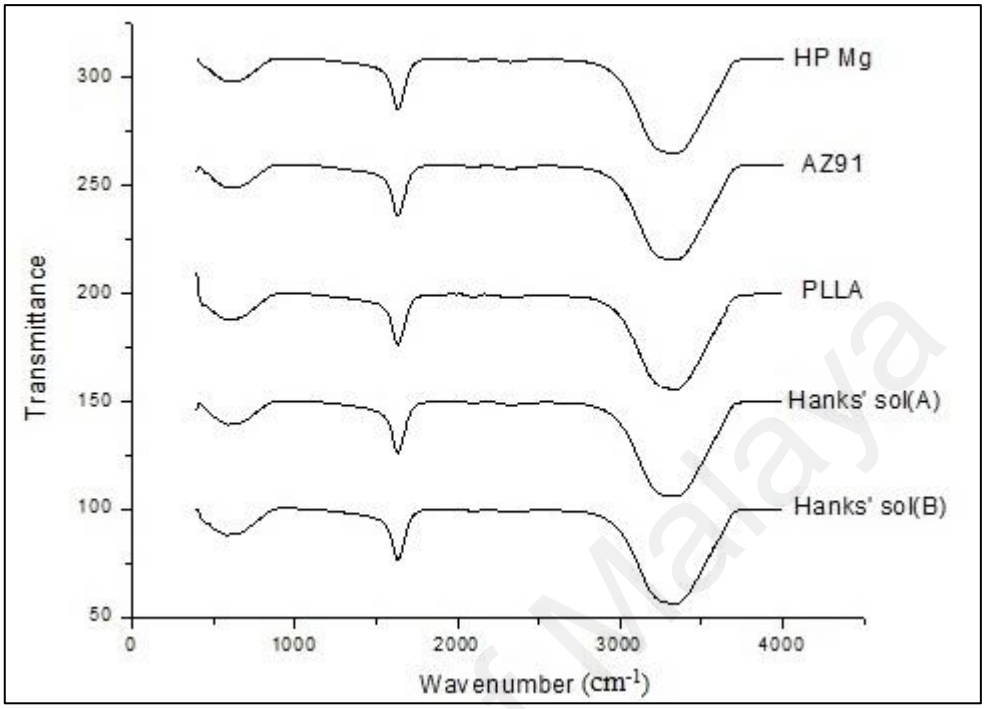

Figure 4.14: FTIR on Hank's solution before and after immersion test.

Figure 4.14 shows FTIR spectrum of Hanks' solution before (Hank's sol (B)) and after (Hank's sol (A)) immersion test. The Hank's solution before immersion test were compared with Hank's solution after 14 days of immersion test without any sample (standard) and with sample such as PLLA, HP Mg and AZ91. There were no significant different in term of peaks. The broad transmittance bands at around 3250 cm^{-1} represented –OH bond which indicate the presence of H_2O in the Hank's solution. The transmittance peak at 1610 cm^{-1} identified as carboxylate (salt) peak. The peak below 1000 cm^{-1} was determined as sodium or phosphorus. The peak of Hank's solutions after immersion test with or without sample are similar with Hank's solution before immersion test (Heacock & Marion, 1956; Miller & Wilkins, 1952). It proved that all corrosion products were attached to the sample throughout the immersion test. It did not leave any trace in the Hank's solution after 14 days of immersion test.

4.3.5 Corroded Surface Evaluation

Figure 4.15 presents the surface appearance after corrosion product removal. Figure 4.15a presents the surface condition of HP Mg. Figure 4.15b presents the surface appearance of AZ91. Figure 4.15c presents the surface appearance of PLLA-HP Mg and Figure 4.15d presents the surface of specimen PLLA-AZ91 after 14 days immersion in Hank's solution.

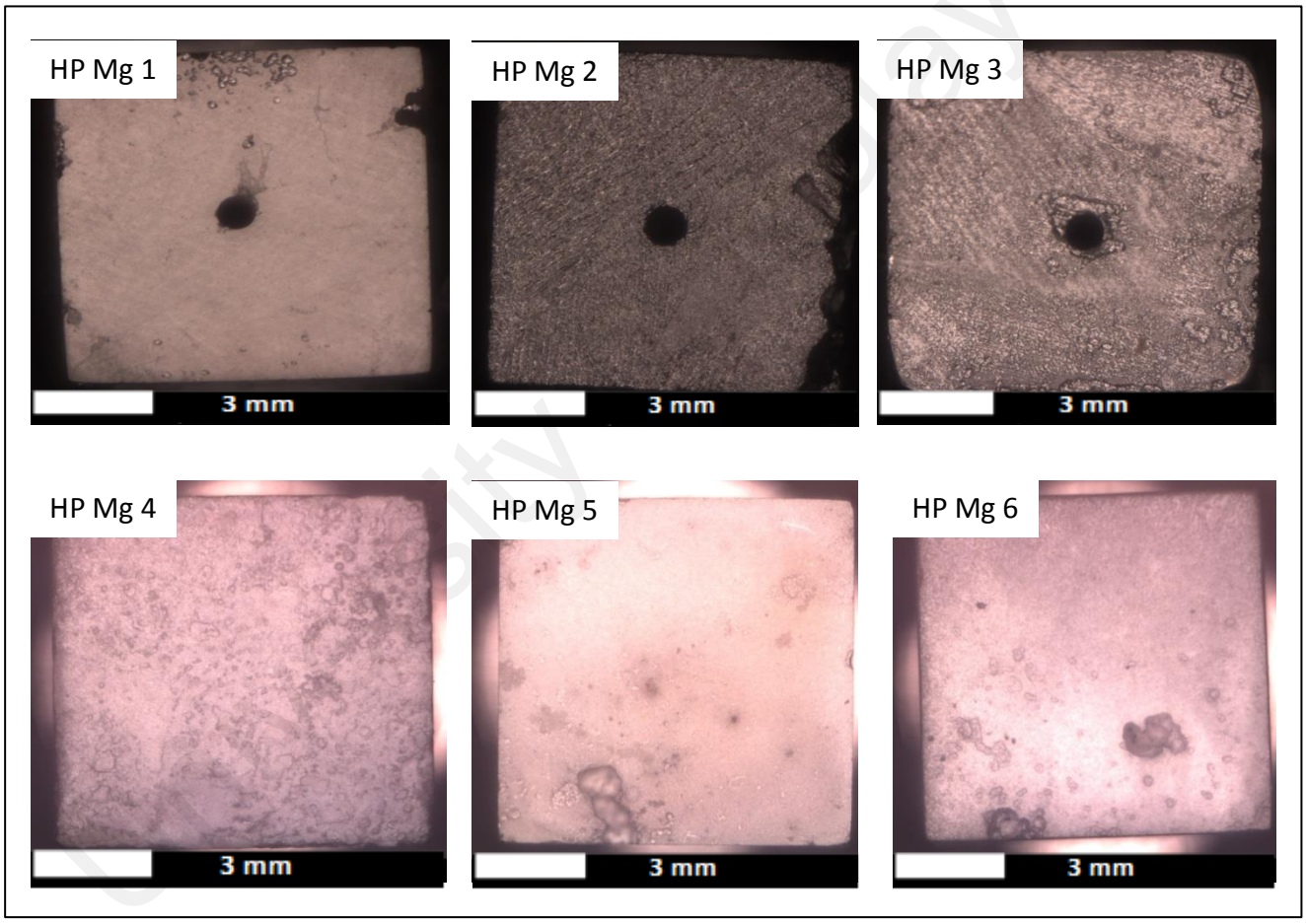

Figure 4.15a: SEM corroded surface of HP Mg after immersion test for 14 days and after removal of corrosion product.

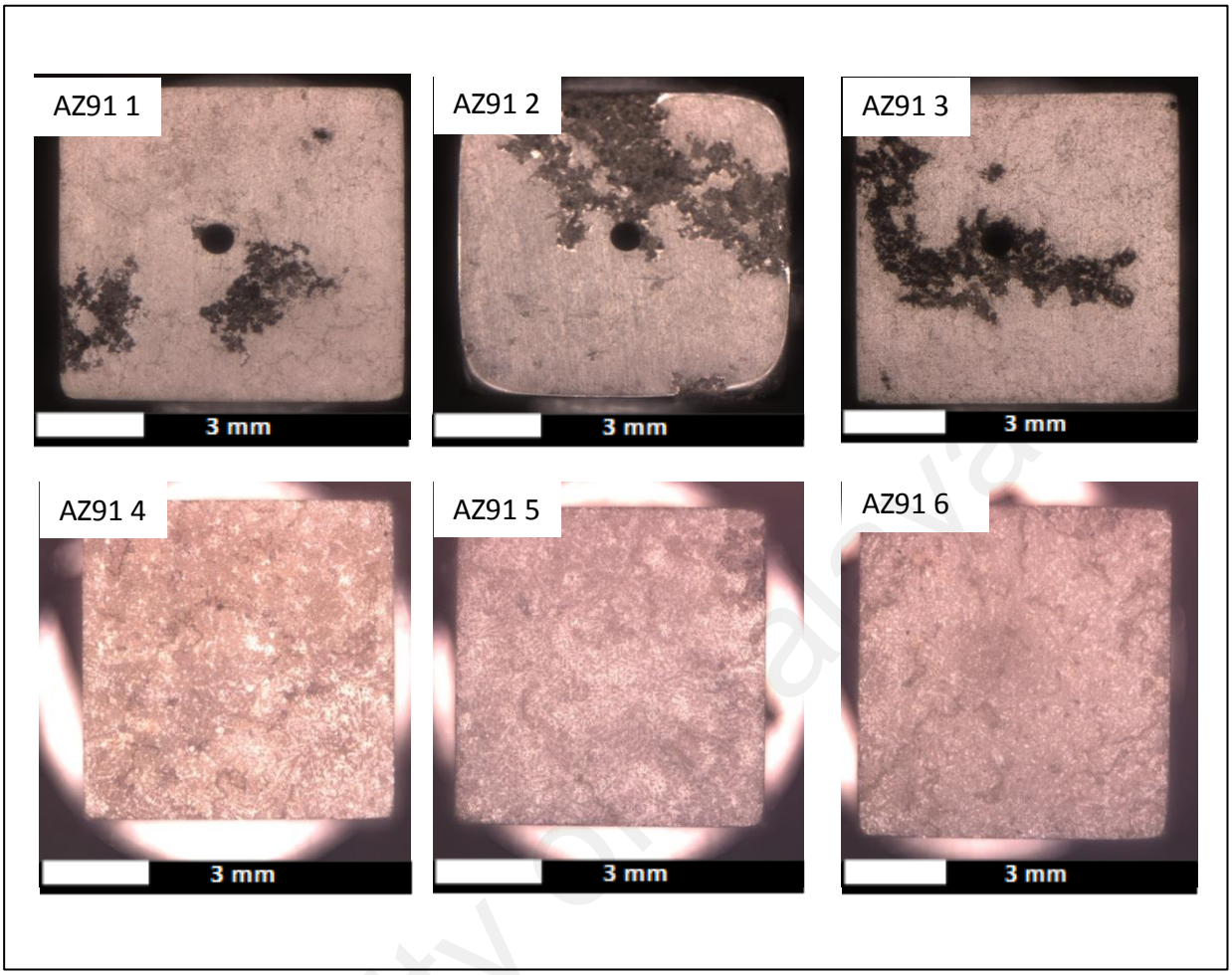

Figure 4.15b: SEM corroded surface of AZ91 after immersion test for 14 days and after removal of corrosion product.

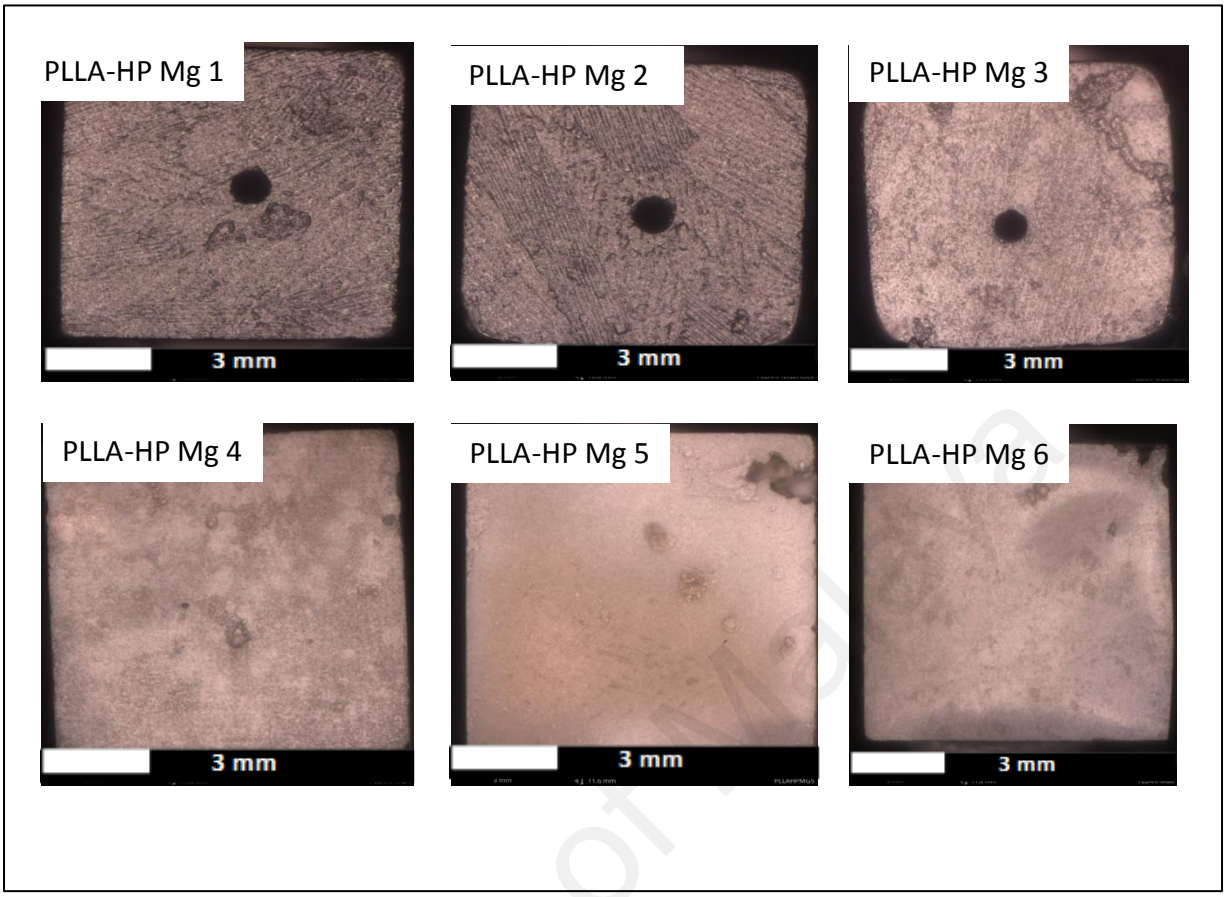

Figure 4.15c: SEM corroded surface of PLLA-HP Mg after immersion test for 14 days and after removal of corrosion product.

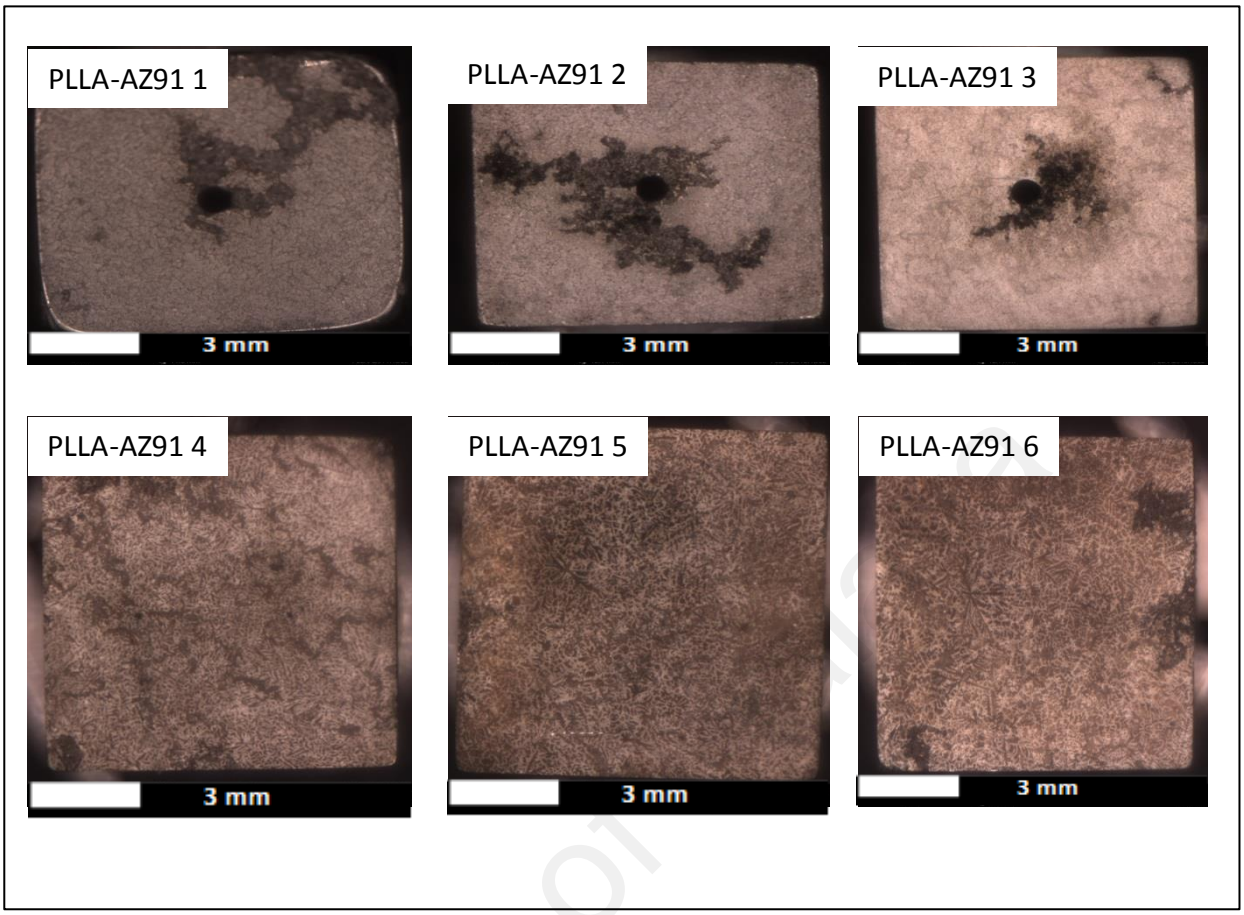

Figure 4.15d: SEM corroded surface of PLLA-AZ91 after immersion test for 14 days and after removal of corrosion product.

From Figure 4.15a, the surface of most uncoated HP Mg samples showed heterogeneous corrosion, severely corroded areas that were adjacent to the samples edge especially HP Mg 2. This indicated that substrate suffered shallow localized corrosion (Xu & Yamamoto, 2012b). The surface appearance of HP Mg 4 which had shown incubation period has superficial corrosion over the sample surface and deep heterogenous corrosion in a several area while some pitting happened on the surface of HP Mg 5 and HP Mg 6. This results were also reported by (Witecka, Bogucka, et al., 2016; Witte, 2015).

Uncoated samples of AZ91 with hole (Figure 4.15b) undergone similar amount of somewhat deeper localized corrosion known as pitting corrosion (Witte et al., 2006). The pitting was started at hole in the centre then spread over the surface. These happened to sample AZ91 2 and AZ91 3. The surface appearance of uncoated AZ91 without hole (AZ91 4, AZ91 5 and AZ91 6) show similar appearance with heterogenous corrosion having spread over sample surface.

For coated samples with hole PLLA-HP Mg 1 and PLLA-HP Mg 2 (Figure 4.15c), fewer flaws and tiny corrosion pits are observed on the cleaned surface as corrosion resistant coating should setback initiation of biodegradation while for PLLA-HP Mg 3 tiny pitting started at the edge of sample. Sample PLLA-HP Mg 3 suffered crevice corrosion. Sample coated without hole, PLLA-HP Mg 4, 5 and 6 underwent heterogenous corrosion which deeper pit was seen on the edge of sample. The coating enable inhibit or avoid localized corrosion while generating degradation on the surface of Mg (Atrens, Liu, & Abidin, 2011).

For samples PLLA-AZ91 with hole; PLLA-AZ91 1, PLLA-AZ91 2 and PLLA-AZ91 3 (Figure 4.15d), there was pitting beneath the PLLA layer in which it started from the hole. For PLLA-AZ91 4, 5 and 6, sample underwent filiform corrosion. This

observation also stated by research work done by (Alabbasi, Liyanaarachchi, & Kannan, 2012). After removal of PLLA layer after 14 days immersion test, it can be seen that some flakes pattern formed on the sample's surface. This is due to water slipped in between fibers of PLLA layer to reach into Mg surface. For the corrosion that happened to the coated samples with hole, it should note that Mg samples degradation happened at places where the coating was destroyed.

From the figures, it is obvious that the crevice corrosion started at hole and spread to the other area. The appearances of coated and uncoated HP Mg after corrosion product removal obtained from this research are similar with previous study (Rojaee, Fathi, & Raeissi, 2013b; Zainal Abidin et al., 2015; L. Zhao, Liu, Wang, Yang, & Liu, 2014). In general, several corrosions were found from the samples used such as localized corrosion, pitting corrosion, filiform corrosion and crevice corrosion.

4.4 PLLA Coating

The behavior of PLLA immersed in Hank's solution at 37ºC for 14 days was also determined by H_2 gas evolution and weight loss rate. These evaluation was done to determine either PLLA layer will inhibit or exhibit the Mg corrosion. Figure 4.16 presents the hydrogen evolution of PLLA immersed in Hank's solution. In this figure, open symbol as hydrogen evolution volume and full symbols for corresponding pH of the solution. Triplicate samples were used; PLLA 1, PLLA 2 and PLLA 3. The hydrogen evolution volume increased with the immersion time.

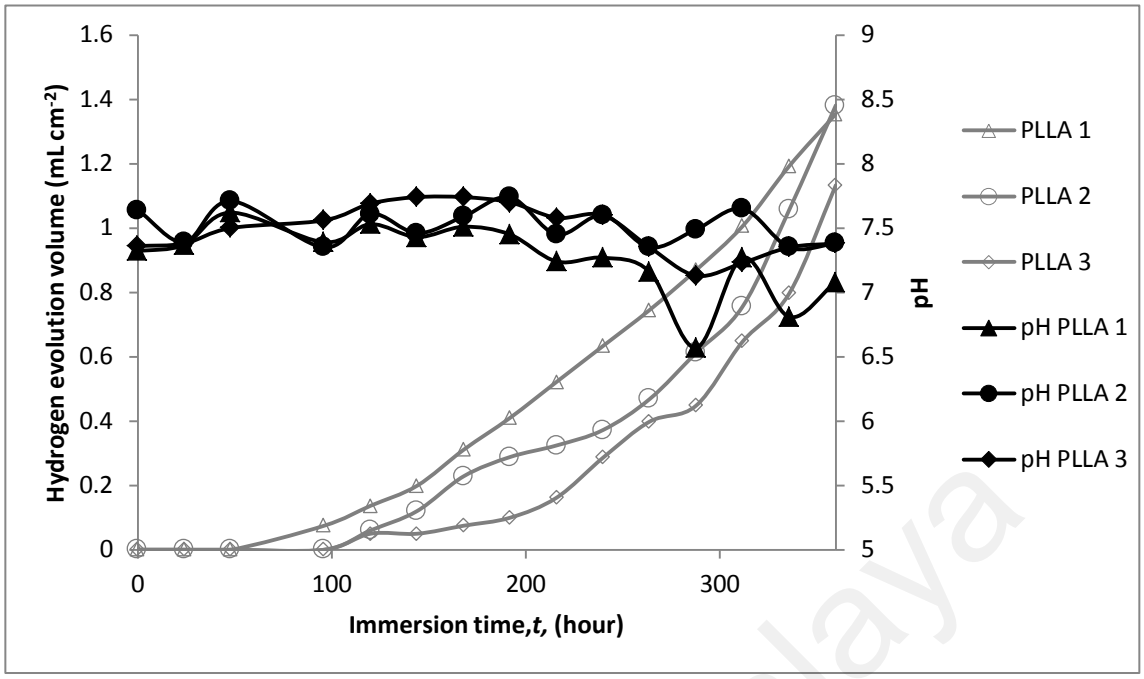

Figure 4.16: Hydrogen evolution of PLLA in Hank's solution for 14 days.

All samples have incubation period in which PLLA 1 was incubated until 50 hr while PLLA 2 and PLLA 3 were in incubation period until 100 hr before increased rapidly until 1.38 ml/cm^2. The incubation period of PLLA and PLLA coated Mg were same, this proved that PLLA layer prevent the degradation of Mg at the beginning of the immersion test (Witecka, Yamamoto, Idaszek, Chlanda, & Święszkowski, 2016). The hydrogen evolution of PLLA samples was too low. In other word, PLLA does not affect the volume of hydrogen evolution of Mg samples in immersion test.

Figure 4.16 also plot the solution pH during the immersion test was done. The full symbols shown on the graph referred to the pH value. The pH was approximately constant during each test. The pH was within 6.81 -7.74. By bubbling CO_2 with partial pressure of 0.009 atm into Hank's solution, the pH was successfully maintained.

Table 4.6: Corrosion rate of PLLA in Hank's solution

Material	Immersion period (hour)		W_L (mg cm^{-2} d^{-1})	P_W (mm y^{-1})	V_{TH} (mL cm^{-2} d^{-1})	P_{AH} (mm d^{-1})
PLLA	1	336	0.0033	0.0069	0.0967	0.2204
	2	336	0.0028	0.0059	0.0987	0.2250
	3	336	0.0012	0.0024	0.0809	0.1840

Table 4.6 shows the weight loss data, $W_{L,}$ the corresponding corrosion rate, P_W, the hydrogen evoluation rate, V_{TH}, and the corresponding corrosion rate, P_{AH} for samples of PLLA in Hank's solution for 14 days. The result of the average corrosion rates showed that the average corrosion rate from the volume of hydrogen evolution were larger than the corrosion rates collected from the weight loss for all samples. The weight loss of PLLA samples was too low. It means there were no significant degradation from the layer (Kim et al., 2003).

CHAPTER 5: CONCLUSIONS AND RECOMMENDATIONS

5.1 Conclusions

In this study, high purity magnesium Mg (HP Mg) and AZ91 have been successfully coated with poly-L-lactic acid (PLLA) by electrospinning method. The PLLA was diluted in chloroform and parameters used for electrospinning; applied voltage 10 kV, distance tip to collector 15 cm and feed rate 1 ml/hr have successfully formed nanofibers PLLA on the surface of magnesium. The Mg surface coated with PLLA was identified by X-ray diffraction, Fourier transform infrared spectrometer (FTIR) and SEM-EDX. From XRD spectrum, the amorphous peaks of PLLA on Mg surface are consistent with previous literature. The transmittance bands of PLLA from FTIR are similar with the standard reference. SEM-EDX reveals the image of PLLA fibers on the Mg surface, thus nanofibers' diameter also determined.

Another principle of this work was to study the corrosion behavior of coated and uncoated HP Mg and AZ91 in Hank's solution. The corrosion evaluation of Mg immersed in Hank's solution for 14 days was determined by hydrogen gas evolution, weight loss rate and SEM-EDX. For all samples, the volume of hydrogen evolution increased with immersion time. The corrosion rates of PLLA-HP Mg without hole was succesfully decreased by 84% while the corrosion rates of PLLA-AZ91 without hole has decreased to about 70%. The samples of PLLA-HP Mg with hole were unable to lower the corrosion rate. However, the corrosion rates of PLLA-AZ91 with hole shown different outcomes which the corrosion rates had decreased to about 76%. From this study, several corrosions were found from the samples such as localized corrosion, pitting corrosion, filiform corrosion and crevice corrosion. Another finding that had been found from this study was the overall corrosion rate of Mg samples with hole can

be ranked as: HP Mg < PLLA-AZ91 < PLLA-HP Mg < AZ91. The corrosion rate of Mg samples without hole is ranked as: PLLA-HP Mg < PLLA-AZ91 < HP Mg < AZ91.

In general, from these results, coated samples without hole had successfully provided protective layer in delaying the corrosion of Mg alloys.

5.2 Recommendations

In the future research, further investigation can be conducted as follows:

i. Different biodegradable polymers such as poly (lactic-co-glycolic acid) (PLGA), polycaprolactone (PCL) and poly (vinyl alcohol) (PVA) can be used to compare with poly (L-lactic acid) (PLLA) on lowering the corrosion rate of Mg and at the same time to produce excellent biocompatibility coating in order to make more feasible and desirable medical implant.
ii. The corrosion behavior of coated and uncoated magnesium in Hank's balanced solution should be longer than 14 days in providing more accurate and reliable results.
iii. The research can be extended by performing in vivo test for the PLLA-Mg samples.
iv. Samples for in vitro and in vivo tests need to be designed appropriately as in all surfaces need to be coated completely and uniformly.

REFERENCES

Abdal-hay, A., Barakat, N. A., & Lim, J. K. (2013). Hydroxyapatite-doped poly (lactic acid) porous film coating for enhanced bioactivity and corrosion behavior of AZ31 Mg alloy for orthopedic applications. *Ceramics International, 39*(1), 183-195.

Abdal-hay, A., Barakat, N. A., & Lim, J. K. (2013). Influence of electrospinning and dip-coating techniques on the degradation and cytocompatibility of Mg-based alloy. *Colloids and Surfaces A: Physicochemical and Engineering Aspects, 420*, 37-45.

Abdal-hay, A., Dewidar, M., Lim, J., & Lim, J. K. (2014). Enhanced biocorrosion resistance of surface modified magnesium alloys using inorganic/organic composite layer for biomedical applications. *Ceramics International, 40*(1), 2237-2247.

Abdal-hay, A., Dewidar, M., & Lim, J. K. (2012). Biocorrosion behavior and cell viability of adhesive polymer coated magnesium based alloys for medical implants. *Applied Surface Science, 261*, 536-546.

Abdal-hay, A., Hwang, M. G., & Lim, J. K. (2012). In vitro bioactivity of titanium implants coated with bicomponent hybrid biodegradable polymers. *Journal of sol-gel science and technology*, *64*(3), 756-764.

Abdal-hay, A., Tijing, L. D., & Lim, J. K. (2013). Characterization of the surface biocompatibility of an electrospun nylon 6/CaP nanofiber scaffold using osteoblasts. *Chemical Engineering Journal, 215*, 57-64.

Agarwal, S., Wendorff, J. H., & Greiner, A. (2008). Use of electrospinning technique for biomedical applications. *Polymer, 49*(26), 5603-5621.

Agrawal, C., & Ray, R. (2001). Biodegrable polymeric scaffolds for musculoskeletal tissue engineering. *J Biomed Mater Res, 55*, 141-150.

Alabbasi, A., Liyanaarachchi, S., & Kannan, M. B. (2012). Polylactic acid coating on a biodegradable magnesium alloy: An in vitro degradation study by electrochemical impedance spectroscopy. *Thin Solid Films, 520*(23), 6841-6844.

Amalina, M. A., Hajime, N., Hideki, Y., Yoshiharu, K., & Shigeyuki, N. (2009). Fabrication of aligned Poly(L-lactide) fibers by electrospinning and drawing. *Macromolecular materials and engineering, 294*, 658-665.

Ambat, R., Aung, N. N., & Zhou, W. (2000). Evaluation of microstructural effects on corrosion behaviour of AZ91D magnesium alloy. *Corrosion Science, 42*(8), 1433-1455.

Armentano, I., Dottori, M., Fortunati, E., Mattioli, S., & Kenny, J. (2010). Biodegradable polymer matrix nanocomposites for tissue engineering: a review. *Polymer Degradation and Stability, 95*(11), 2126-2146.

Atrens, A., Liu, M., & Abidin, N. I. Z. (2011). Corrosion mechanism applicable to biodegradable magnesium implants. *Materials Science and Engineering: B, 176*(20), 1609-1636.

Azad, A.-M., McKelvey, S., & Al-Firdaus, Z. (2008). Fabrication of antimicrobial titania nanofibers by electrospinning. *Advanced Materials, Manufacturing, and Testing Information Analysis Center, 3*(3), 2-7.

Bajgai, M. P., Parajuli, D. C., Park, S. J., Chu, K. H., Kang, H. S., & Kim, H. Y. (2011). Hydroxyapatite particulate nanofiber modified Titanium: In-vitro bioactivity. *Bioceramics Development and Applications, 1*. doi:10.4303/bda/D110131

Bergsma, J. E., Rozema, F., Bos, R., Boering, G., De Bruijn, W., & Pennings, A. (1995). In vivo degradation and biocompatibility study of in vitro pre-degraded as-polymerized polylactide particles. *Biomaterials, 16*(4), 267-274.

Berzina-Cimdina, L., & Borodajenko, N. (2012). Research of calcium phosphates using Fourier transform infrared spectroscopy *Infrared Spectroscopy-Materials Science, Engineering and Technology*: InTech.

Cai, Q., Xu, Q., Feng, Q., Cao, X., Yang, X., & Deng, X. (2011). Biomineralization of electrospun poly (l-lactic acid)/gelatin composite fibrous scaffold by using a supersaturated simulated body fluid with continuous CO 2 bubbling. *Applied Surface Science, 257*(23), 10109-10118.

Cao, F., Shi, Z., Song, G.-L., Liu, M., & Atrens, A. (2013). Corrosion behaviour in salt spray and in 3.5% NaCl solution saturated with Mg (OH) 2 of as-cast and solution heat-treated binary Mg–X alloys: X= Mn, Sn, Ca, Zn, Al, Zr, Si, Sr. *Corrosion Science, 76*, 60-97.

Castellani, C., Lindtner, R. A., Hausbrandt, P., Tschegg, E., Stanzl-Tschegg, S. E., Zanoni, G., . . . Weinberg, A.-M. (2011). Bone–implant interface strength and osseointegration: Biodegradable magnesium alloy versus standard titanium control. *Acta Biomaterialia, 7*(1), 432-440.

Chaya, A., Yoshizawa, S., Verdelis, K., Myers, N., Costello, B. J., Chou, D.-T., . . . Sfeir, C. (2015). In vivo study of magnesium plate and screw degradation and bone fracture healing. *Acta Biomaterialia, 18*, 262-269.

Chen, X. N., Gu, Y. X., Lee, J. H., Lee, W. Y., & Wang, H. J. (2012). Multifunctional surfaces with biomimetic nanofibres and drug-eluting micro-patterns for infection control and bone tissue formation. *European Cells and Materials, 24*, 237-248.

Chen, J.-P., & Su, C.-H. (2011). Surface modification of electrospun PLLA nanofibers by plasma treatment and cationized gelatin immobilization for cartilage tissue engineering. *Acta Biomaterialia, 7*(1), 234-243.

Chen, J., Song, Y., Shan, D., & Han, E.-H. (2015). Influence of alloying elements and microstructure on the formation of hydrotalcite film on Mg alloys. *Corrosion Science, 93*, 90-99.

Chen, Y., Wan, G., Wang, J., Zhao, S., Zhao, Y., & Huang, N. (2013). Covalent immobilization of phytic acid on Mg by alkaline pre-treatment: Corrosion and degradation behavior in phosphate buffered saline. *Corrosion Science, 75*, 280-286.

Chou, D.-T., Hong, D., Saha, P., Ferrero, J., Lee, B., Tan, Z., . . . Kumta, P. N. (2013). In vitro and in vivo corrosion, cytocompatibility and mechanical properties of biodegradable Mg–Y–Ca–Zr alloys as implant materials. *Acta Biomaterialia, 9*(10), 8518-8533.

Chronakis, I. S. (2005). Novel nanocomposites and nanoceramics based on polymer nanofibers using electrospinning process—a review. *Journal of Materials Processing Technology*, *167*(2), 283-293.

Chu, P. K., Chen, J., Wang, L., & Huang, N. (2002). Plasma-surface modification of biomaterials. *Materials Science and Engineering: R: Reports*, *36*(5), 143-206.

Croisier, F., & Jérôme, C. (2013). Chitosan-based biomaterials for tissue engineering. *European Polymer Journal*, *49*(4), 780-792.

Dargaville, B. L., Vaquette, C., Rasoul, F., Cooper-White, J. J., Campbell, J. H., & Whittaker, A. K. (2013). Electrospinning and crosslinking of low-molecular-weight poly (trimethylene carbonate-co-l-lactide) as an elastomeric scaffold for vascular engineering. *Acta Biomaterialia*, *9*(6), 6885-6897.

Deitzel, J., Kleinmeyer, J., Harris, D., & Beck, T. N. (2001). The effect of processing variables on the morphology of electrospun nanofibers and textiles. *Polymer*, *42*, 261-272.

Dhanapal, A., Boopathy, S. R., & Balasubramanian, V. (2012). Influence of pH value, chloride ion concentration and immersion time on corrosion rate of friction stir welded AZ61A magnesium alloy weldments. *Journal of Alloys and Compounds*, *523*, 49-60.

Dixit, S., Singh, S. R., Yilma, A. N., Agee, R. D., Taha, M., & Dennis, V. A. (2014). Poly (lactic acid)–poly (ethylene glycol) nanoparticles provide sustained delivery of a Chlamydia trachomatis recombinant MOMP peptide and potentiate systemic adaptive immune responses in mice. *Nanomedicine: Nanotechnology, Biology and Medicine*, *10*(6), 1311-1321.

Dorozhkin, S. V. (2014). Calcium orthophosphate coatings on magnesium and its biodegradable alloys. *Acta Biomaterialia*, *10*(7), 2919-2934.

Doshi, J., & Reneker, D. H. (1995). Electrospinning process and applications of electrospun fibers. *Journal of electrostatics*, *35*(2-3), 151-160.

Duan, Y., Wang, Z., Yan, W., Wang, S., Zhang, S., & Jia, J. (2007). Preparation of collagen-coated electrospun nanofibers by remote plasma treatment and their biological properties. *Journal of Biomaterials Science, Polymer Edition, 18*(9), 1153-1164.

Elias, C. N., Oshida, Y., Lima, J. H. C., & Muller, C. A. (2008). Relationship between surface properties (roughness, wettability and morphology) of titanium and dental implant removal torque. *Journal of the mechanical behavior of biomedical materials, 1*(3), 234-242.

Fang, J., Wang, X., & Lin, T. (2011). *Functional applications of electrospun nanofibers*: InTech–Open Access Publisher.

Fischer, J., Pröfrock, D., Hort, N., Willumeit, R., & Feyerabend, F. (2011). Improved cytotoxicity testing of magnesium materials. *Materials Science and Engineering: B, 176*(11), 830-834. doi: https://doi.org/10.1016/j.mseb.2011.04.008

Frenot, A., & Chronakis, I. S. (2003). Polymer nanofibers assembled by electrospinning. *Current opinion in colloid & interface science, 8*(1), 64-75.

G. Kister, G. Cassanas, & M. Vert. (1998). Effects of morphology, conformation and configuration on the IR and Raman spectra of various poly(lactic acid)s. *Polymer, 39*(2), 267-273.

Gu, Y., Bandopadhyay, S., Chen, C.-f., Ning, C., & Guo, Y. (2013). Long-term corrosion inhibition mechanism of microarc oxidation coated AZ31 Mg alloys for biomedical applications. *Materials & Design, 46*, 66-75.

Guo, B., Glavas, L., & Albertsson, A.-C. (2013). Biodegradable and electrically conducting polymers for biomedical applications. *Progress in Polymer Science, 38*(9), 1263-1286.

Guo, L., & Li, H. (2004). Fabrication and characterization of thin nano-hydroxyapatite coatings on titanium. *Surface and Coatings Technology, 185*(2), 268-274.

Gupta, B., Revagade, N., & Hilborn, J. (2007). Poly (lactic acid) fiber: an overview. *Progress in Polymer Science, 32*(4), 455-482.

Hänzi, A. C., Gerber, I., Schinhammer, M., Löffler, J. F., & Uggowitzer, P. J. (2010). On the in vitro and in vivo degradation performance and biological response of new biodegradable Mg–Y–Zn alloys. *Acta Biomaterialia, 6*(5), 1824-1833.

Heacock, R., & Marion, L. (1956). The infrared spectra of secondary amines and their salts. *Canadian Journal of Chemistry, 34*(12), 1782-1795.

Hiromoto, S. (2015). Self-healing property of hydroxyapatite and octacalcium phosphate coaatings on pure magnesium and magnesium alloy. *Corrosion Science, 100*, 284-294.

Hiromoto, S., Yamamoto, A., Maruyama, N., Somekawa, H., & Mukai, T. (2008). Influence of pH and flow on the polarisation behaviour of pure magnesium in borate buffer solutions. *Corrosion Science, 50*(12), 3561-3568.

Hornberger, H., Virtanen, S., & Boccaccini, A. (2012). Biomedical coatings on magnesium alloys–a review. *Acta Biomaterialia, 8*(7), 2442-2455.

Hort, N., Huang, Y., Fechner, D., Störmer, M., Blawert, C., Witte, F., . . . Kainer, K. (2010). Magnesium alloys as implant materials–principles of property design for Mg–RE alloys. *Acta Biomaterialia, 6*(5), 1714-1725.

Iafisco, M., Foltran, I., Sabbatini, S., Tosi, G., & Roveri, N. (2012). Electrospun nanostructured fibers of collagen-biomimetic apatite on titanium alloy. *Bioinorganic chemistry and applications, 2012*.

Jacobs, J. J., Gilbert, J. L., & Urban, R. M. (1998). Corrosion of metal orthopaedic implants. *JBJS, 80*(2), 268-282.

Jiang, W., Cheng, J., & Dinesh, K. (2009). *Improved mechanical properties of nanocrystalline hydroxyapatite coating for dental and orthopedic implants.* Paper presented at the Mater Res Soc.

Jönsson, M., Persson, D., & Thierry, D. (2007). Corrosion product formation during NaCl induced atmospheric corrosion of magnesium alloy AZ91D. *Corrosion Science, 49*(3), 1540-1558.

Khajavi, R., & Abbasipour, M. (2012). Electrospinning as a versatile method for fabricating coreshell, hollow and porous nanofibers. *Scientia Iranica, 19*(6), 2029-2034.

Kim, K., Yu, M., Zong, X., Chiu, J., Fang, D., Seo, Y.-S., . . . Hadjiargyrou, M. (2003). Control of degradation rate and hydrophilicity in electrospun non-woven poly (D, L-lactide) nanofiber scaffolds for biomedical applications. *Biomaterials, 24*(27), 4977-4985.

Krikorian, V., & Pochan, D. J. (2003). Poly (L-lactic acid)/layered silicate nanocomposite: fabrication, characterization, and properties. *Chemistry of materials, 15*(22), 4317-4324.

Kister, G., Cassanas, G., & Vert, M. (1998). Effects of morphology, conformation and configuration on the IR and Raman spectra of various poly (lactic acid) s. *Polymer, 39*(2), 267-273.

Lamaka, S., Vaghefinazari, B., Mei, D., Petrauskas, R., Höche, D., & Zheludkevich, M. (2017). Comprehensive screening of Mg corrosion inhibitors. *Corrosion Science*.

Levit, K., Wier, L., Stranges, E., Ryan, K., & Elixhauser, A. (2009). HCUP facts and figures: statistics on hospital-based care in the United States, 2007. *Rockville, MD: Agency for Healthcare Research and Quality*.

Li, W.-J., Cooper, J. A., Mauck, R. L., & Tuan, R. S. (2006). Fabrication and characterization of six electrospun poly (α-hydroxy ester)-based fibrous scaffolds for tissue engineering applications. *Acta Biomaterialia, 2*(4), 377-385.

Li, Y., Lee, I.-S., Cui, F.-Z., & Choi, S.-H. (2008). The biocompatibility of nanostructured calcium phosphate coated on micro-arc oxidized titanium. *Biomaterials, 29*(13), 2025-2032.

Liang, D., Hsiao, B. S., & Chu, B. (2007). Functional electrospun nanofibrous scaffolds for biomedical applications. *Advanced Drug Delivery Reviews, 59*(14), 1392-1412.

Lim, L.-T., Auras, R., & Rubino, M. (2008). Processing technologies for poly (lactic acid). *Progress in Polymer Science, 33*(8), 820-852.

Luo, C., Nangrejo, M., & Edirisinghe, M. (2010). A novel method of selecting solvents for polymer electrospinning. *Polymer, 51*(7), 1654-1662.

Ma, J., Thompson, M., Zhao, N., & Zhu, D. (2014). Similarities and differences in coatings for magnesium-based stents and orthopaedic implants. *Journal of orthopaedic translation, 2*(3), 118-130.

Ma, Z., Chen, F., Zhu, Y.-J., Cui, T., & Liu, X.-Y. (2011). Amorphous calcium phosphate/poly (D,L-lactic acid) composite nanofibers: Electrospinning preparation and biomineralization. *Journal of Colloid and Interface Science*(359), 371-379.

Ma, Z., Mao, Z., & Gao, C. (2007). Surface modification and property analysis of biomedical polymers used for tissue engineering. *Colloids and Surfaces B: Biointerfaces, 60*(2), 137-157.

Mendonça, G., Mendonça, D. B., Aragao, F. J., & Cooper, L. F. (2008). Advancing dental implant surface technology–from micron-to nanotopography. *Biomaterials, 29*(28), 3822-3835.

Miller, F. A., & Wilkins, C. H. (1952). Infrared spectra and characteristic frequencies of inorganic ions. *Analytical Chemistry, 24*(8), 1253-1294.

Min, B.-M., You, Y., Kim, J.-M., Lee, S. J., & Park, W. H. (2004). Formation of nanostructured poly (lactic-co-glycolic acid)/chitin matrix and its cellular response to normal human keratinocytes and fibroblasts. *Carbohydrate Polymers, 57*(3), 285-292.

Ngiam, M., Liao, S., Patil, A. J., Cheng, Z., Chan, C. K., & Ramakrishna, S. (2009). The fabrication of nano-hydroxyapatite on PLGA and PLGA/collagen nanofibrous composite scaffolds and their effects in osteoblastic behavior for bone tissue engineering. *Bone, 45*(1), 4-16.

Niu, J., Yuan, G., Liao, Y., Mao, L., Zhang, J., Wang, Y., . . . Ding, W. (2013). Enhanced biocorrosion resistance and biocompatibility of degradable Mg–Nd–Zn–Zr alloy by brushite coating. *Materials Science and Engineering: C, 33*(8), 4833-4841.

Nudelman, F., Lausch, A. J., Sommerdijk, N. A., & Sone, E. D. (2013). In vitro models of collagen biomineralization. *Journal of structural biology, 183*(2), 258-269.

Ostrowski, N., Lee, B., Enick, N., Carlson, B., Kunjukunju, S., Roy, A., & Kumta, P. N. (2013). Corrosion protection and improved cytocompatibility of biodegradable polymeric layer-by-layer coatings on AZ31 magnesium alloys. *Acta Biomaterialia, 9*(10), 8704-8713.

Pandey, A., Pandey, G. C., & Aswath, P. B. (2008). Synthesis of polylactic acid–polyglycolic acid blends using microwave radiation. *Journal of the mechanical behavior of biomedical materials, 1*(3), 227-233.

Pardo, A., Merino, M., Coy, A., Viejo, F., Arrabal, R., & Feliú, S. (2008). Influence of microstructure and composition on the corrosion behaviour of Mg/Al alloys in chloride media. *Electrochimica Acta, 53*(27), 7890-7902.

Pei, L.-Z., Yin, W.-Y., Wang, J.-F., Chen, J., Fan, C.-G., & Zhang, Q.-F. (2010). Low temperature synthesis of magnesium oxide and spinel powders by a sol-gel process. *Materials Research, 13*(3), 339-343.

Porter, R., Kaplan, J., Homeier, B., & Beers, M. (1995). Merk manual of diagnosis and therapy (chapter 12) Endocrine & metabolic disorders (section 2): Water, electrolyte mineral and acid/base metabolism: Whitehouse Station: Merck & Co. Inc.

Qiao, Z., Shi, Z., Hort, N., Zainal Abidin, N. I., & Atrens, A. (2012). Corrosion behaviour of a nominally high purity Mg ingot produced by permanent mould direct chill casting. *Corrosion Science, 61*, 185-207.

Rahmany, M. B., & Van Dyke, M. (2013). Biomimetic approaches to modulate cellular adhesion in biomaterials: A review. *Acta Biomaterialia, 9*(3), 5431-5437.

Ravichandran, R. (2009). *Biomimetic surface modification of dental implant for enhanced osseointegration* (Doctoral dissertation).

Razavi, M., Fathi, M., Savabi, O., Razavi, S. M., Beni, B. H., Vashaee, D., & Tayebi, L. (2014). Controlling the degradation rate of bioactive magnesium implants by electrophoretic deposition of akermanite coating. *Ceramics International, 40*, 3865-3872.

Rojaee, R., Fathi, M., & Raeissi, K. (2013a). Controlling the degradation rate of AZ91 magnesium alloy via sol-gel derived nanostructured hydroxyapatite coating. *Materials Science and Engineering C, 33*, 3817-3825.

Rojaee, R., Fathi, M., & Raeissi, K. (2013b). Electrophoretic deposition of nanostructured ydroxyapatite coating on AZ91 magnesium alloy implants with different surface treatments. *Applied Surface Science, 285P*, 664-673.

Shah, P. N., Manthe, R. L., Lopina, S. T., & Yun, Y. H. (2009). Electrospinning of L-tyrosine polyurethanes for potential biomedical applications. *Polymer, 50*(10), 2281-2289.

Shenoy, S. L., Bates, W. D., Frisch, H. L., & Wnek, G. E. (2005). Role of chain entanglements on fiber formation during electrospinning of polymer solutions: good solvent, non-specific polymer–polymer interaction limit. *Polymer, 46*(10), 3372-3384.

Shi, P., Niu, B., Shanshan, E., Chen, Y., & Li, Q. (2015). Preparation and characterization of PLA coating and PLA/MAO composite coatings on AZ31 magnesium alloy for improvement of corrosion resistance. *Surface and Coatings Technology, 262*, 26-32.

Shi, Z., & Atrens, A. (2011). An innovative specimen configuration for the study of Mg corrosion. *Corrosion Science, 53*, 226-246.

Singer, F., Distler, T., & Virtanen, S. (2014). Long-term corrosion behavior of poly-l-lactic acid coated magnesium in dulbecco's modified eagle medium at body temperature. *Int. J. Electrochem. Sci, 9*, 7965-7976.

Song, G. (2007). Control of biodegradation of biocompatable magnesium alloys. *Corrosion Science, 49*(4), 1696-1701.

Song, G., & Song, S. (2007). A possible biodegradable magnesium implant material. *Advanced Engineering Materials, 9*(4), 298-302.

Song, Y. W., Shan, D. Y., & Han, E. H. (2008). Electrodeposition of hydroxyapatite coating on AZ91D magnesium alloy for biomaterial application. *Materials letters, 62*(17), 3276-3279.

Staiger, M. P., Pietak, A. M., Huadmai, J., & Dias, G. (2006). Magnesium and its alloys as orthopedic biomaterials: a review. *Biomaterials, 27*(9), 1728-1734.

Sui, J., & Cai, W. (2006). Effect of diamond-like carbon (DLC) on the properties of the NiTi alloys. *Diamond and related materials, 15*(10), 1720-1726.

Sun, B., Long, Y. Z., Zhang, H. D., Li, M. M., Duvail, J. L., Jiang, X. Y., & Yin, H. L. (2014). Advances in three-dimensional nanofibrous macrostructures via electrospinning. *Progress in Polymer Science, 39*, 862-890.

Tan, S., Inai, R., Kotaki, M., & Ramakrishna, S. (2005). Systematic parameter study for ultra-fine fiber fabrication via electrospinning process. *Polymer, 46*(16), 6128-6134.

Tie, D., Feyerabend, F., Mueller, W.-D., Schade, R., Liefeith, K., Kainer, K. U., & Willumeit, R. (2012). Antibacterial biodegradable Mg-Ag alloys. *European cells & materials, 25*, 284-298; discussion 298.

Tian, H., Tang, Z., Zhuang, X., Chen, X., & Jing, X. (2012). Biodegradable synthetic polymers: preparation, functionalization and biomedical application. *Progress in Polymer Science, 37*(2), 237-280.

Troitskii, V., & Tsitrin, D. (1944). The resorbing metallic alloy 'Osteosinthezit'as material for fastening broken bone. *Khirurgiia, 8*(1), 41-44.

Virtanen, S. (2011). Biodegradable Mg and Mg alloys: Corrosion and biocompatibility. *Materials Science and Engineering: B, 176*(20), 1600-1608.

Wang, H.-S., Fu, G.-D., & Li, X.-S. (2009). Functional polymeric nanofibers from electrospinning. *Recent Patents on Nanotechnology, 3*, 21-31.

Wang, Z., & Guo, Y. (2016). Corrosion resistance and adhesion of poly (L-lactic acid)/MgF2 composite coating on AZ31 magnesium alloy for biomedical application. *Russian Journal of Non-Ferrous Metals, 57*(4), 381-388.

Wen, C., Guan, S., Peng, L., Ren, C., Wang, X., & Hu, Z. (2009). Characterization and degradation behavior of AZ31 alloy surface modified by bone-like hydroxyapatite for implant applications. *Applied Surface Science, 255*(13), 6433-6438.

Witecka, A., Bogucka, A., Yamamoto, A., Máthis, K., Krajňák, T., Jaroszewicz, J., & Święszkowski, W. (2016). In vitro degradation of ZM21 magnesium alloy in simulated body fluids. *Materials Science and Engineering: C, 65*, 59-69.

Witecka, A., Yamamoto, A., Idaszek, J., Chlanda, A., & Święszkowski, W. (2016). Influence of biodegradable polymer coatings on corrosion, cytocompatibility and cell functionality of Mg-2.0 Zn-0.98 Mn magnesium alloy. *Colloids and Surfaces B: Biointerfaces, 144*, 284-292.

Witte, F. (2015). Reprint of: The history of biodegradable magnesium implants: A review. *Acta Biomaterialia, 23*, S28-S40.

Witte, F., Hort, N., Vogt, C., Cohen, S., Kainer, K. U., Willumeit, R., & Feyerabend, F. (2008). Degradable biomaterials based on magnesium corrosion. *Current opinion in solid state and materials science, 12*(5), 63-72.

Witte, F. (2015). Reprint of: The history of biodegradable magnesium implants: A review. *Acta Biomaterialia, 23*, S28-S40.

Witte, F., Fischer, J., Nellesen, J., Crostack, H.-A., Kaese, V., Pisch, A., . . . Windhagen, H. (2006). In vitro and in vivo corrosion measurements of magnesium alloys. *Biomaterials, 27*(7), 1013-1018.

Wong, H. M., Yeung, K. W., Lam, K. O., Tam, V., Chu, P. K., Luk, K. D., & Cheung, K. M. (2010). A biodegradable polymer-based coating to control the performance of magnesium alloy orthopaedic implants. *Biomaterials, 31*(8), 2084-2096.

Xu, L., Pan, F., Yu, G., Yang, L., Zhang, E., & Yang, K. (2009). In vitro and in vivo evaluation of the surface bioactivity of a calcium phosphate coated magnesium alloy. *Biomaterials, 30*(8), 1512-1523.

Xu, L., & Yamamoto, A. (2012a). Characteristics and cytocompatibility of biodegradable polymer film on magnesium by spin coating. *Colloids and Surfaces B: Biointerfaces, 93*, 67-74.

Xu, L., & Yamamoto, A. (2012b). In vitro degradation of biodegradable polymer-coated magnesium under cell culture condition. *Applied Surface Science, 258*(17), 6353-6358.

Xu, L., Yu, G., Zhang, E., Pan, F., & Yang, K. (2007). In vivo corrosion behavior of Mg-Mn-Zn alloy for bone implant application. *Journal of Biomedical Materials Research Part A, 83*(3), 703-711.

Yamamoto, A., & Hiromoto, S. (2009). Effect of inorganic salts, amino acids and proteins on the degradation of pure magnesium in vitro. *Materials Science and Engineering C, 29*, 1559-1568.

Yu, K., Chen, L., Zhao, J., Li, S., Dai, Y., Huang, Q., & Yu, Z. (2012). In vitro corrosion behavior and In vivo biodegradation of biomedical β-Ca 3 (PO 4) 2/Mg–Zn composites. *Acta Biomaterialia, 8*(7), 2845-2855.

Zainal Abidin, N. I., Forno, A. D., Bestetti, M., Martin, D., Beer, A., & Atrens, A. (2015). Evaluation of coating for Mg Alloys for Biomedical applications. *Advanced Engineering Materials, 17*, 58-67.

Zainal Abidin, N. I., Atrens, A. D., Martin, D., & Atrens, A. (2011). Corrosion of high purity Mg, Mg2Zn0.2Mn, ZE41 and AZ91 in Hank's solution at 37'C. *Corrosion Science, 53*, 3542-3556.

Zainal Abidin, N. I., Martin, D., & Atrens, A. (2011). Corrosion of high purity Mg, AZ91, ZE41 and Mg2Zn0.2Mn in Hank's solution at room temperature. *Corrosion Science, 53*(3), 862-872. doi: https://doi.org/10.1016/j.corsci.2010.10.008

Zainal Abidin, N. I., Rolfe, B., Owen, H., Malisano, J., Martin, D., Hofstetter, J., . . . Atrens, A. (2013). The in vivo and in vitro corrosion of high-purity magnesium and magnesium alloys WZ21 and AZ91. *Corrosion Science, 75*, 354-366.

Zhang, Q., Mochalin, V. N., Neitzel, I., Hazeli, K., Niu, J., Kontsos, A., . . . Gogotsi, Y. (2012). Mechanical properties and biomineralization of multifunctional nanodiamond-PLLA composites for bone tissue engineering. *Biomaterials, 33*(20), 5067-5075.

Zhang, R., & Ma, P. X. (1999). Porous poly (L-lactic acid)/apatite composites created by biomimetic process.

Zhao, D., Wang, T., Nahan, K., Guo, X., Zhang, Z., Dong, Z., . . . Kumta, P. N. (2017). In vivo characterization of magnesium alloy biodegradation using electrochemical H 2 monitoring, ICP-MS, and XPS. *Acta Biomaterialia, 50*, 556-565.

Zhao, M. C., Liu, M., Song, G., & Atrens, A. (2008). Influence of the β-phase morphology on the corrosion of the Mg alloy AZ91. *Corrosion Science*, *50*(7), 1939-1953.

Zhao, M. C., Schmutz, P., Brunner, S., Liu, M., Song, G., & Atrens, A. (2009). An exploratory study of the corrosion of mg alloys during interrupted salt spray testing. *Corrosion Science, 51*, 1277-1292.

Zreiqat, H., Howlett, C., Zannettino, A., Evans, P., Schulze-Tanzil, G., Knabe, C., & Shakibaei, M. (2002). Mechanisms of magnesium-stimulated adhesion of osteoblastic cells to commonly used orthopaedic implants. *Journal of Biomedical Materials Research Part A, 62*(2), 175-184.

LIST OF PUBLICATIONS AND PAPERS PRESENTED

1. Wan Nur Atikah Haji Wan Nafi, presented "Electrospun Nanostructured Fibers of Biobased Polymer on Magnesium", 2nd International Conference on the Science and Engineering of Materials on 16-18 November 2015 at Kuala Lumpur.

2. Atikah Wan Nafi, Amalina, M. A., Zainal Abidin, N. I., Noor Hidayah Abdul Aziz & Katayoon Kalantari (In press). Effect Study of Poly L-lactic acid on the Corrosion of Coated Magnesium in Hanks' Solution. *Sains Malaysiana*.